

## Article

# Catalog of Geomagnetic Storms with Dst Index $\leq -50$ nT and Their Solar and Interplanetary Origin (1996–2019)

Rositsa Miteva <sup>1,\*</sup>  and Susan W. Samwel <sup>2</sup> 

<sup>1</sup> Institute of Astronomy and National Astronomical Observatory (IANAO)—Bulgarian Academy of Sciences, 1784 Sofia, Bulgaria

<sup>2</sup> National Research Institute of Astronomy and Geophysics (NRIAG), Helwan, Cairo 11421, Egypt; samwelsw@nriag.sci.eg

\* Correspondence: rmiteva@nao-rozhen.org

**Abstract:** We present a comprehensive catalog of geomagnetic storms (GSs) with a Dst index  $\leq -50$  nT detected during solar cycles (SCs) 23 and 24 (1996–2019). About 550 events were identified in the Kyoto database and used as a starting point for this study. The solar origin of the GSs, in terms of coronal mass ejections (CMEs), solar flares (SFs), and in situ-observed energetic particles, was identified where possible using temporal constraints and wide Earth-directed ejecta. In addition, any accompanied interplanetary (IP) sources, such as ICMEs and IP shock waves detected at 1 AU, are also considered. The resulting occurrence rates and correlation plots are presented and discussed in the space weather framework.

**Keywords:** geomagnetic storms; (interplanetary) coronal mass ejections; interplanetary shock waves; solar flares; energetic particles; space weather



**Citation:** Miteva, R.; Samwel, S.W. Catalog of Geomagnetic Storms with Dst Index  $\leq -50$  nT and Their Solar and Interplanetary Origin (1996–2019). *Atmosphere* **2023**, *14*, 1744. <https://doi.org/10.3390/atmos14121744>

Academic Editors: Aibing Zhang and Lei Li

Received: 31 October 2023

Revised: 19 November 2023

Accepted: 24 November 2023

Published: 27 November 2023



**Copyright:** © 2023 by the authors. Licensee MDPI, Basel, Switzerland. This article is an open access article distributed under the terms and conditions of the Creative Commons Attribution (CC BY) license (<https://creativecommons.org/licenses/by/4.0/>).

## 1. Introduction

The term geomagnetic storm (GS) is used to describe, in general, a significant disruption in Earth's magnetosphere, driven by structures in the solar wind [1]. The concept was proposed for the first time by Alexander von Humboldt as magnetic storms, in order to describe and link between the rapid magnetic declination variations and the appearance of the Northern Lights phenomena [2]. This ground-based disturbance intensifies and prolongs when a prevalent southward-directed magnetic field ( $B_z$ ) is present [3].

The fundamental cause of these storms lies in the magnetic interaction between a planetary magnetosphere and the interplanetary magnetic field (IMF) [4]. A GS is a phenomenon of energy transfer between (ejecta in) the solar wind and the terrestrial magnetosphere based on the mechanism of magnetic reconnection [1]. The latter process is sufficiently effective when the IMF of the plasma structure is southward-directed [5]. During the reconnection, solar wind plasma is injected and transported to the night-side magnetosphere. However, the protons drift to the west, whereas the electrons to the east, thus forming a 'ring current' around the Earth. It is this current that eventually causes a sharp decrease in the magnetic field measured by ground-based stations [6].

The strongest GSs occur when coronal mass ejections (CMEs) are expelled in the Earth direction, arrive at 1 AU as soon as about 12–13 h (based on the fastest ejecta ever recorded) and up to 5–6 days later (based on typical slow solar wind speed). These are termed interplanetary (IP) CMEs or ICMEs, creating conditions for magnetic field-line reconnection [5,7–11]. The reliable identification of (I)CME geoeffectiveness is a topic of ongoing research [12].

There are other recognized sources of the geomagnetic disturbances predominantly driven by fast solar wind streams and occasionally repeating with the solar rotation (termed recurrent GSs). Such structures are the high-speed streams (HSSs), crossings of the helio-

spheric current sheet, and corotating interaction regions (CIRs) [12]. The resulting GSs are often of weaker intensity, but longer in duration.

The effects by ICMEs/IP shocks and HSSs/CIRs are also responsible for different effects on the terrestrial radiation belts [13], whereas fast variations of the magnetic field vector are currently linked to geomagnetically induced currents (GICs) in ground-based conduction systems [14,15], which subsequently may cause transformer damages. On the other hand, the Starlink satellite failure in February 2022 happened during the course of a weak GS [16] with the exact reasons still being debatable, e.g., see [17] and the references therein. Novel techniques, such as machine learning algorithms for the classification of GSs, are also being tested [18].

In general, the GS progresses through three phases. It commences with a sudden compression of the magnetosphere due to an increase in the dynamic pressure of the solar wind. This phase, known as sudden storm commencement (SSC), is characterized by an abrupt positive variation of the disturbance storm time (Dst) index. The subsequent phase is referred to as the main phase. Here, the Dst index takes negative values during the injection of energized plasma in the equatorial ring current, ultimately reaching its minimum value. This is followed by the recovery phase, wherein particle transport into the ring current decelerates, enabling various loss processes to diminish ring current particle fluxes to their quiet-time level. This process is reflected by the Dst values, which start to rise until they return to pre-sudden commencement levels, signifying the restoration of the geomagnetic field to pre-storm levels [3,4,19].

Various indices are used to measure the GS intensity (see, e.g., <https://www.ngdc.noaa.gov/stp/geomag/indices.html>, accessed on 26 November 2023), and the commonly used ones are listed below:

- Dst is a geomagnetic index that measures the magnitude of the GSs. It is calculated based on the average value of the horizontal component of the Earth's magnetic field. The intensity is expressed in negative values and measured in nano-Teslas [20–22]. This index is directly related to the total kinetic energy of the ring current particles and the overall energetics of the GS. The Sym-H index is the 1 min resolution of Dst index.
- The Kp (planetary) index quantifies the disturbance of the horizontal component of Earth's magnetic field due to geomagnetic activity. It ranges from 0 to 9, with higher values indicating more-severe disturbances [23,24].
- The Ap (planetary) index is another measure of geomagnetic activity, representing the planetary averaged amplitude of the magnetic field. It provides a daily average value [25].
- The Auroral Electrojet (AE) index measures the level of geomagnetic activity in the auroral zone. It is also used as an indication of the strength of the GS [26].
- The AA index is a global index of magnetic activity from the K indices of two nearly antipodal magnetic observatories in England and Australia. Its variation, the AA index, is the three-hourly equivalent amplitude antipodal index.
- Other indices or variations of the above ([https://isgi.unistra.fr/indices\\_asy.php](https://isgi.unistra.fr/indices_asy.php), accessed on 26 November 2023).

There is no unique definition of the strength of the GSs concerning the Dst index, as the thresholds differ between different authors (the amplitude of the Dst index will preferably be used in the text): moderate ( $50 \leq |Dst| < 100$  nT), intense ( $100 \leq |Dst| < 250$  nT), and super-storms ( $|Dst| \geq 250$  nT) were introduced by [3]; intense  $|Dst| \geq 100$  nT and super-intense  $|Dst| \geq 500$  nT were proposed by [27]; many teams use the term 'major' for  $|Dst| \geq 100$  nT; whereas the strongest GSs on record (following the Carrington–Hodgson event on 1–2 September 1859) are named 'extreme' [28]. A combination between two indices was proposed by [3,24], where the GSs are categorized into weak ( $30 < |Dst| < 50$  nT, with  $0 \leq Kp \leq 5$ ), moderate ( $50 < |Dst| < 100$  nT, with  $5 < Kp < 7$ ), and intense ( $|Dst| > 100$  nT, with  $7 \leq Kp \leq 9$ ).

Alternatively, NASA employs the NOAA Space Weather Scale (<https://www.swpc.noaa.gov/noaa-scales-explanation>, accessed on 26 November 2023) to categorize the in-

tensity of GSs. Known as the G-scale, it spans from G1, denoting minor storms, to G5, representing extreme events. A G1 storm, classified as minor, may result in slight fluctuations in power grids and minor disruptions to satellite operations. A G2 storm, categorized as moderate, can trigger voltage alarms in power systems, potential transformer damage, and increased drag on low Earth orbit satellites. G3 storms, characterized as strong, have the potential to induce voltage control issues, transformer damage, and satellite surface charging. Severe G4 storms can lead to widespread voltage control problems, transformer damage, and satellite surface charging. In the most-extreme cases, G5 storms can lead to a complete collapse of power systems, prolonged surface charging of satellites, and even damage to pipeline systems. The engineering aspects of this scale impressively demonstrate the importance of the GSs (and their precursors) to space weather research [29]. The term space weather is considered here in a broader framework of all direct and indirect influences of the solar activity phenomena on the terrestrial atmospheric layers, technology, and human safety [30]. A focused study on the space weather effects (including the strength and structure of GSs) on satellite operations was recently compiled [17].

A rich volume of research has been devoted to the GS phenomenon, e.g., see [27,31,32] for literature reviews, since a representative description goes beyond the scope of this report. For example, very early on, it was established that the Dst index varies with the conditions in the IP space [33], and the topic continued to be further explored with the availability of new satellite data, e.g., [7,34]. Recent studies over two solar cycles (SCs) confirm the stronger trends between the Dst and the IP parameters compared to solar eruptive phenomena. Namely, a recent study [35] explored the Pearson correlations between 111 GSs with  $|Dst| \geq 100$  nT and a variety of physical parameters in SC23 and 24, confirming strong relationships with total B-field, the product between solar wind speed and the  $B_z$ -component and the ICME speed. Moderate correlations are reported with the solar wind speed and pressure and weak/no clear correlation with plasma density, solar flare (SF) class, CME speed and angular width (AW), and the fluxes and fluences of energetic particles. Over the same time period, another study [32] extended the list of GSs with  $|Dst| \geq 50$  nT to 179 in SC23 and 85 in SC24 or a reduction of 47% of the GS activity being present. They reported correlations between several GS indices (SymH, Kp, and AE) with solar wind speed, IMF  $B_z$ , and their product and confirmed the high correlations in SC23, but not in SC24.

In order to explore the statistical relationship, a list of GSs needs to be compiled with carefully identified parent solar and/or accompanied IP activity. Lists of historical GSs can be found in [36,37]. Examples of major GSs ( $|Dst| > 100$  nT) generated by CIRs were presented by [38], another study in SC24 was completed by [39], but no list was provided, whereas 12 cases in 1996–2016 were reported by [40]. Due to the lack of a comprehensive listing covering the period of interest for our study, we will not consider the effects of CIRs separately.

Previous catalogs of GSs considered SC23 or earlier time periods and have been reported in the past with a different focus: to search for solar and IP origin of major ( $|Dst| > 100$  nT) GSs [41]; to study the 50 most intense in the Dst index GSs [42]; to explore extreme GSs [36]. An important aspect of any follow-up studies is the ability to compare the results. This is impeded to a degree when no catalog is provided, as in the case of the recently completed statistical analysis with the IP parameters covering SC23 and 24 by [32].

The aim of this study was to provide an open-access catalog of GSs with a Dst index  $\leq -50$  nT, together with their solar and IP sources in SC23 and 24 (1996–2019). We upgraded a previous study focused on SC24 [43] and propose a source identity based on an association study between the GS peaks and the timing and physical properties of the IP structures and CMEs. The here presented GSs can be additionally affected by HSSs/CIRs, which was not accounted for with the performed analyses. In contrast, a set of criteria was applied on the entire list of GSs, resulting in certain/uncertain associations. Our catalog aims to serve as a basis of a living document with additions and

corrections being periodically implemented, e.g., filtering out a possible contamination by CIRs, especially for the weaker GSs. The online version of the list will be supported at <https://catalogs.astro.bas.bg/> (accessed on 26 November 2023).

## 2. Methodology

### 2.1. Data

In order to characterize the strength of the GS storm, we used the Dst index provided by the World Data Center for Geomagnetism, Kyoto: <https://wdc.kugi.kyoto-u.ac.jp/dst/dir/index.html> (accessed on 26 November 2023). The final values of the Dst index are currently available through the end of 2016, whereas for the period 2017–2019 of our list, we used the provisional ones; however, only minor changes in the Dst index were expected. Based on the visual inspection of the monthly Dst-curves and to the best of our abilities, we identified 546 GSs where the Dst value dropped below the adopted threshold for this study of  $-50$  nT, as reported to the nearest hour. No identification of the onset and end times of each GS was attempted by us; instead, we focused on the amplitude of the Dst index. For the purposes of this statistical analysis, pre-event disturbances were also not considered. However, we noticed that the identity of 49 GSs seemed to be compromised due to a previous event or an extended turbulent period according to our assessment. These GSs are denoted as ‘uncertain’ in our list.

Apart from the Dst index, we collected the readily provided characteristics of ICMEs, IP shock waves, CMEs, and in situ-observed energetic particles, using data from various spacecraft positioned at the Lagrangian point L1 or at geostationary orbit for the SFs.

The speeds of the ICMEs observed close to Earth have been already identified and reported in several sources. A catalog of ICME timing and characteristics based on Wind satellite data is provided at: [https://wind.nasa.gov/ICME\\_catalog/ICME\\_catalog\\_viewer.php](https://wind.nasa.gov/ICME_catalog/ICME_catalog_viewer.php) (accessed on 26 November 2023). An alternative ICME catalog using data from the ACE satellite can be found here: <https://izw1.caltech.edu/ACE/ASC/DATA/level3/icmetable2.htm> (accessed on 26 November 2023). We preferred the latter, as the catalog gives also the solar origin (i.e., the parent CMEs) for some of the ICMEs.

The timing and speeds of IP shocks using Wind observations are given in great detail by <https://lweb.cfa.harvard.edu/shocks/> (accessed on 26 November 2023), where we used the median reported value for the shock speed. Alternative sources for IP shocks, both from the Wind and ACE spacecraft, can be found at <http://www.ipshocks.fi/database> (accessed on 26 November 2023); however, due to some temporary access interruptions, we could not use this database for our study.

The properties of the CMEs were collected from the well-known CDAW SOHO/LASCO database [https://cdaw.gsfc.nasa.gov/CME\\_list/](https://cdaw.gsfc.nasa.gov/CME_list/) (accessed on 26 November 2023). The following parameters were adopted: timing (first occurrence above the occulting disk); linear speed, i.e., the on-sky projected speed, obtained by fitting a straight line to the height–time measurements of the fastest segment of the leading edge of the CME; AW, i.e., the sky-plane width of CMEs, which is typically measured in the field of view between 1.5 and 6 solar radii; and the measurement position angle (MPA), as measured from the north and advancing in the counterclockwise direction. Both AW and MPA are reported in degrees.

In order to quantify the geomagnetic effects due to phenomena (e.g., electromagnetic emissions or particles) originating at the same solar eruption, SFs and solar energetic particles are also considered. These are the ones physically related to the already identified CME eruption. The SF information was taken from a GOES-based list with the timing, soft X-ray (SXR) class, and helio-locations: <https://www.ngdc.noaa.gov/stp/space-weather/solar-data/solar-features/solar-flares/x-rays/goes/xrs/> (accessed on 26 November 2023). For the case of the in situ-observed particles, e.g., protons (SEPs) and electrons (SEEs), we compared their associated CMEs and SFs (identified previously) with the GS-associated CMEs and SFs in our list. The matching cases were selected, and only the peak particle fluxes were used here, as provided by the respective catalogs: Wind/EPACT SEP catalog <http://www.stil.bas.bg/SEPcatalog/> (accessed on 26 November 2023) (19–28 MeV) and

ACE/EPAM SEE catalog [https://www.nriag.sci.eg/ace\\_electron\\_catalog/](https://www.nriag.sci.eg/ace_electron_catalog/) (accessed on 26 November 2023) (103–175 keV), reported in [44] and [45], respectively.

## 2.2. Association Procedure

When associating the IP counterpart of a GS, we only employed timing constraints. The travel time of the disturbance first detected at L1 to the magnetosphere was estimated to be within one hour, depending on the speed. Since we did not quantitatively evaluate the onset time of the GSs, but used their peak times instead, we needed to allow for a wider time window between the hour of the minimum Dst and its driver at L1. Namely, we searched for an identified ICME and IP shock wave within a 1-day period prior to the GS peak time. Based on this guideline, we could identify 228 ICMEs (or about a 42% of occurrence rate) and 179 IP shock waves (close to 33%, respectively). In the majority of the cases, the IP phenomenon identified by us was a unique candidate.

The following criteria for the search of the solar driver of GSs were used: Starting from the hour of minimum value of the Dst measurement (depicting the GS peak), we isolated 3- and 5-day periods ahead of each GS. These periods cover the characteristic travel time of ejecta from the Sun to Earth. Longer periods are possible, though less probable to cause detectable geomagnetic response. Firstly, in a shorter time period, we looked for Earth-directed ejecta, namely a halo CME (with an AW of 360°), with the fastest candidate being selected. In the case of no candidates, we searched for a halo CME with a speed above 600 km s<sup>-1</sup> in the wider time window. The imposed threshold for the speed was subjective to a degree; however, we kept the requirement as the ejecta should be faster than the typical speeds of the slow solar wind. Furthermore, we set an additional requirement for the AW to be above 90°. This set of criteria (or quality flagging) was applied to the entire GS event list. For the major GSs ( $|Dst| \geq 100$  nT), ~100 cases, we adopted the associations from our previous work [35].

A main source of uncertainty on the solar origin identification followed from the non-fulfillment of the adopted association criteria. As a rule, all proposed associations within a 3-day period were considered as certain, whereas those within a 3- to 5-day period were denoted as uncertain. Any other cases that diverged to a small degree from the above-described criteria were also considered uncertain associations (e.g., the candidate was a non-halo CME with the specified 3-day period, slow CME, or other deviations from the rules, but reported as a GS origin by other online catalogs, as described above). From the entire GS list, we could identify in total 330 CMEs or the occurrence rate of 60%, split into 157 ( $\lesssim 29\%$ ) certain and 173 ( $\gtrsim 31\%$ ) uncertain solar origin associations. The large amount of uncertain CME associations was due to the majority of weak GSs in our list.

Furthermore, we investigated the certain vs. uncertain CME association among the 49 uncertain GSs and obtained 4 vs. 17 cases, respectively (whereas the remaining 28 uncertain GSs had no CME association). Due to the low fraction of uncertain GS-related CMEs, the entire GS distribution will be considered as certain only.

The SF association with GSs was performed via the SF inter-connection to CMEs. The later procedure is relatively easy to complete and was based on the timing (within 1 h) and helio-location (the SF position to be within 90° of the reported MPA of the CME). Thus, concerning the SF as a solar origin, we obtained 227 GSs with an SF or 42%. Based on the certain/uncertain label of the CME, we obtained 118 (22%) certain SFs and 109 (20%) uncertain ones.

From the entire list, only 90 SEPs (16%) and 110 SEEs (20%) could be associated with GSs, based on the reported CMEs and SFs linked to these particles. Since the CMEs played the role of an intermediary here as well, the certain and uncertain labels of the particles were due to certain and uncertain types of CMEs.

For visualization purposes, we used the entire GS sample, or over SC23 and 24. For completeness, we calculated occurrence rates separately for SC23 and SC24. All three considered time periods are summarized in Table A1 in Appendix A.

The IP driver proposed by us and solar origin are not immune to misidentifications and should be regarded as a first approximation only. IP structures such as HSSs and/or CIRs can be the true cause of many of the weaker GSs. For example, a catalog of high-speed streams and GSs is available at <http://www.geodin.ro/varsiti/> (accessed on 26 November 2023), but only during SC24. As already explained above, due to the lack of a consistent list of solar wind streams and their link to GSs over the last two SCs, we will not consider this aspect in our analyses.

Another important and very helpful online tool for inspecting plasma structures in the heliosphere is provided by <http://helioweather.net/archive/> (accessed on 26 November 2023). Again, the coverage was only during SC24, and the information from these simulations could only be applied over a smaller fraction of our list. For the consistency of the association procedure over both SCs, we had to drop this source.

### 3. Results

#### 3.1. Catalog of GSs

The total number of GSs in SC23+24 after our visual identification amounted to 546; see Table A2 in Appendix B; of these, 361 (or 66%) occurred in SC23 and 185 (34%) in SC24, plotted in the left side of Figure 1 using a stacked histogram. The dark-colored bars denote the number of certain events and the fraction of light-gray-colored bars the uncertain GSs. The SC24 was also weaker in terms of GSs with a 51% drop.

The distribution of GSs according to their Dst index is shown in Figure 1 (right) for the entire time period, SC23+24. The strongest GS in our list had a Dst index of  $-422$  nT, whereas the majority of the GSs had  $|Dst| \leq 100$  nT. For better visualization, we used the log<sub>10</sub>-linear format. The power law distribution of the phenomena can be recognized, at least for the weak GSs: when the  $|Dst|$  is between 50 and 200 nT, the magnitude of the slope is  $\lesssim 0.03$ , whereas above 200 nT we notice a flat distribution consisting of a few GSs. At the lower end of the Dst distribution cluster are the uncertain GSs: these GSs had, on average, lower mean and median  $|Dst|$  values (in the range of 57–74 nT) regardless of the time period of interest. The certain GSs, on the other hand, had the same values as for the entire sample (from 66 to 92 nT in absolute values), whereas, for the entire sample (denoted by ‘all’ in the plot), the values were 86/69. All mean and median values are summarized in Table 1 for each of the time periods of interest.

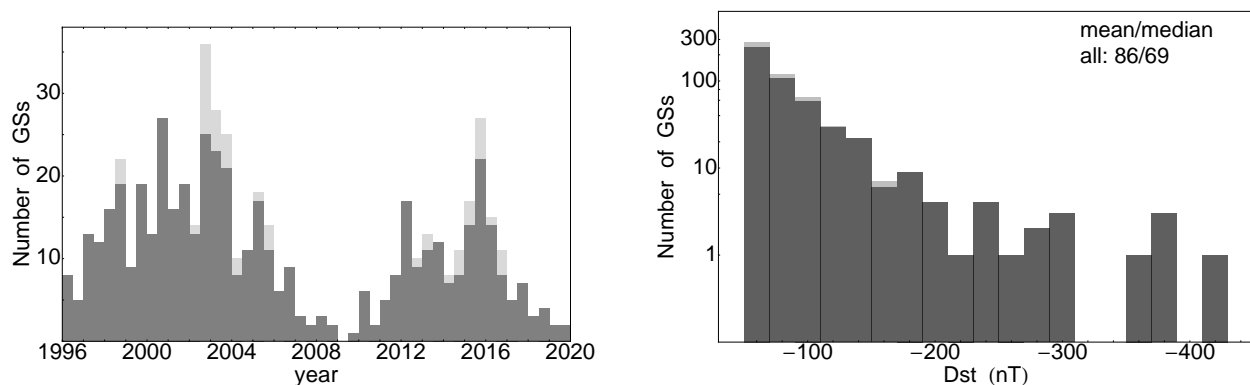


**Figure 1.** Yearly distribution of the GSs on the left (bin width of 0.5 years) and Dst index distribution on the right (bin width 20 nT). Certain events are shown in dark and uncertain in light gray color.

**Table 1.** Mean/median values for the entire sample (given in bold font) and separately for the certain and uncertain categories for each of the considered phenomena denoted by ‘type’. Units: absolute value of Dst in nT; speeds in km s<sup>−1</sup>; SEP flux in differential proton flux units (DPFU) or protons/(cm<sup>2</sup> sr s MeV)<sup>−1</sup>; SEE flux in differential electron flux units (DEFU) or electrons/(cm<sup>2</sup> sr s keV)<sup>−1</sup>. The exact sample size is given in parentheses.

Type	SC23	SC24	SC23+24
<b>GS  Dst </b>	<b>91/71 (361)</b>	<b>75/66 (185)</b>	<b>86/69 (546)</b>
- certain	92/72 (331)	77/67 (166)	87/70 (497)
- uncertain	74/70 (30)	65/57 (19)	71/64 (49)
<b>ICME speed</b>	<b>499/460 (159)</b>	<b>447/440 (69)</b>	<b>483/460 (228)</b>
- certain	495/460 (151)	446/435 (68)	480/450 (219)
- uncertain	575/520 (8)	490 (1)	566/520 (9)
<b>IP shock speed</b>	<b>543/517 (127)</b>	<b>463/445 (52)</b>	<b>520/479 (179)</b>
- certain	537/500 (124)	463/440 (48)	517/478 (172)
- uncertain	787/768 (3)	452/470 (4)	595/497 (7)
<b>CME speed</b>	<b>1037/899 (220)</b>	<b>943/803 (110)</b>	<b>1006/874 (330)</b>
- certain	1123/1004 (114)	2684/987 (43)	1007/1003 (157)
- uncertain	945/833 (106)	866/745 (67)	915/791 (173)
<b>CME AW</b>	<b>278/360 (220)</b>	<b>286/360 (110)</b>	<b>280/360 (330)</b>
- certain	331/360 (114)	353/360 (43)	337/360 (157)
- uncertain	220/182 (106)	243/257 (67)	229/200 (173)
<b>SF class</b>	<b>M1.5/M1.2 (157)</b>	<b>M1.5/M1.8 (70)</b>	<b>M1.5/M1.4 (227)</b>
- certain	M3.1/M3.9 (86)	M2.1/M2.8 (32)	M2.8/M3.5 (118)
- uncertain	C6.4/C5.2 (71)	M1.1/M1.3 (38)	C7.7/C6.7 (109)
<b>SEP flux</b>	<b>0.71/0.61 (57)</b>	<b>0.21/0.14 (33)</b>	<b>0.45/0.31 (90)</b>
- certain	1.19/0.67 (43)	0.35/0.39 (20)	0.80/0.60 (63)
- uncertain	0.14/0.16 (14)	0.10/0.07 (13)	0.12/0.10 (27)
<b>SEE flux (×10<sup>3</sup>)</b>	<b>7.8/9.8 (69)</b>	<b>2.1/1.3 (41)</b>	<b>4.8/4.6 (110)</b>
- certain	13.5/12.4 (51)	2.9/1.3 (23)	8.4/9.5 (74)
- uncertain	1.7/1.2 (18)	1.4/1.0 (18)	1.5/1.2 (36)

### 3.2. IP Origin

For SC23+24, we identified 42% (228/546) ICME events and 33% (179/546) IP shock waves with similar fractions for the ICMEs in each of the two SCs; see Table A1. For completeness, Table 1 gives the mean and median values for the speeds of the GS-associated ICMEs and IP shock waves for the certain, uncertain, and both categories. However, the number of uncertain (according to the GS identity) ICME and IP shocks was minimal. This is why, for the plots and correlations with the IP phenomena, we will not differentiate into two categories. The mean/median values of the entire sample (given in bold font in Table 1) were nearly identical to those of certain categories.

The scatter plots between the speeds and the Dst index are shown in Figures 2 and 3 (left) in the same linear scale for comparison. On the right are shown the histograms for the speeds of the GS-associated phenomena, ICME or IP shock, respectively. A clustering at small values i.e., for the speed at around 500 km s<sup>−1</sup> and for the |Dst| < 100 nT) was evident. The extent of IP shock wave speeds was slightly larger than the range in speeds covered by the ICMEs (after the exclusion of the outlier). The mean/median values of the speeds can be inspected from Table 1. The median values of the ICME and IP shock speeds were similar, 460–480 km s<sup>−1</sup>, whereas the sample of the IP shock speeds had a larger mean value by about 40 km s<sup>−1</sup> compared to the ICME sample (Table 1).

In both cases, there was a rough positive trend in the correlation between the speeds of IP phenomena and the GS strength, as shown in each plot, however not very strong due to the large spread. For quantitative comparison, we used Pearson correlation coefficients, whereas for the uncertainty, we used the bootstrapping method, as described in [44,45]. A slightly better correlation was obtained between the |Dst| and ICME speeds (0.45 ± 0.07), compared to the IP shock speeds (0.31 ± 0.06). The sample size is given in parentheses in

the plots. In terms of the SC trends, the values for the speeds in SC23 tend to be slightly larger than those in SC24, especially for the IP shocks.

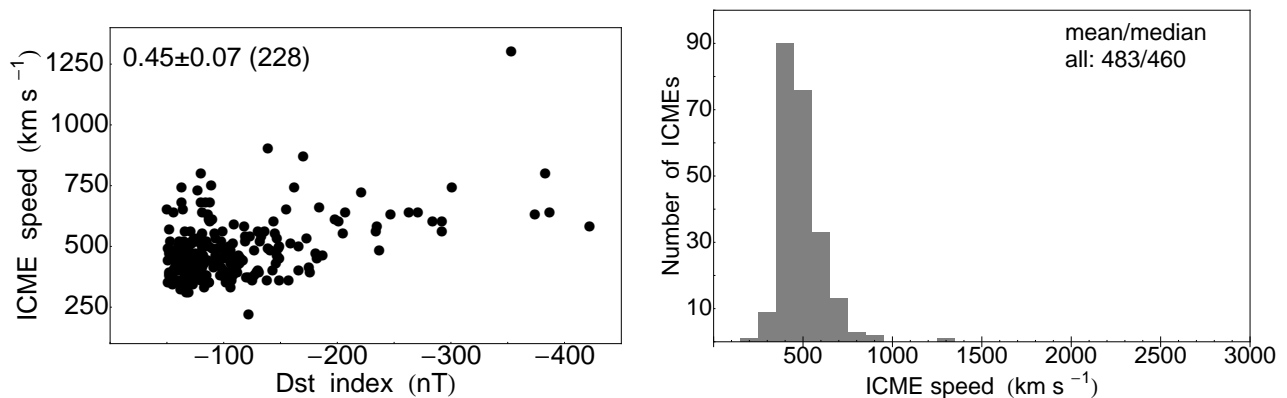


**Figure 2.** Scatter plots between the Dst index (nT) and the ICME speed (on the left) and its distribution (on the right, bin width of  $100 \text{ km s}^{-1}$ ) for the entire event sample.

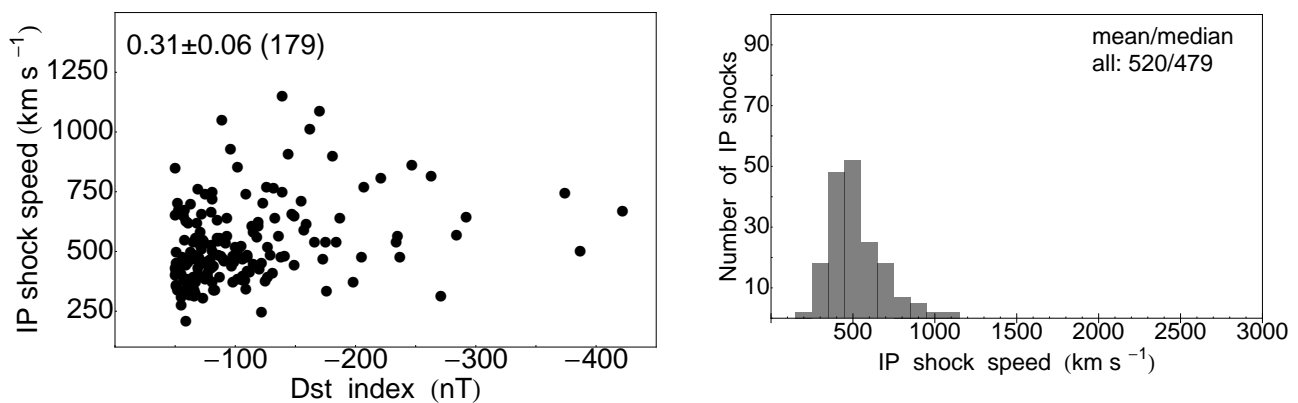


**Figure 3.** Scatter plots between the Dst index (nT) and the IP shock speed (on the left) and its distribution (on the right, bin width of  $100 \text{ km s}^{-1}$ ) for the entire event sample.

### 3.3. Solar Origin

The solar origin of GSs is given via the GS-associated CMEs, SFs, SEPs and SEEs with occurrence rates in SC23+24 as follows, 60%, 42%, 16% and 20%, respectively, with only slight variations (of the order of several percents) between the SCs; see Table A1 for the details. The focal point here is the association of the CMEs, and here, we will recognize certain and uncertain cases. Specifically, Figure 4 shows the scatter plot between the CME linear speed and Dst index (on the left) and the histogram of the CME speed (on the right). Empty circles and light gray color denote uncertain events, whereas filled circles and dark color denote certain events. The uncertain CME associations were concentrated for slower ejecta with mean/median values of  $915/791 \text{ km s}^{-1}$ ; see also Table 1. The mean/median values for the speeds of the certain-type CMEs were around  $1000 \text{ km s}^{-1}$  and were the same as the mean values of the entire CME sample (though the median value for the latter was lower,  $874 \text{ km s}^{-1}$ ).

Overall, no clear correlations could be identified between the GSs and CME speed properties; see Figure 4 (left) for neither of the categories: certain:  $0.18 \pm 0.08$ ; uncertain:  $-0.11 \pm 0.08$ ; all:  $0.17 \pm 0.07$ . The abrupt starting line is due to the threshold selection of  $-50 \text{ nT}$ . Similarly, the relationship with the CME AW is shown in Figure 5 (left), and no correlation with the Dst index was obtained: certain:  $0.07 \pm 0.07$ ; uncertain:  $0.02 \pm 0.07$ ; all:  $0.22 \pm 0.03$ . There was an over-representation of halo CMEs, and the majority of non-halo cases ( $<300$  degrees) were uncertain.

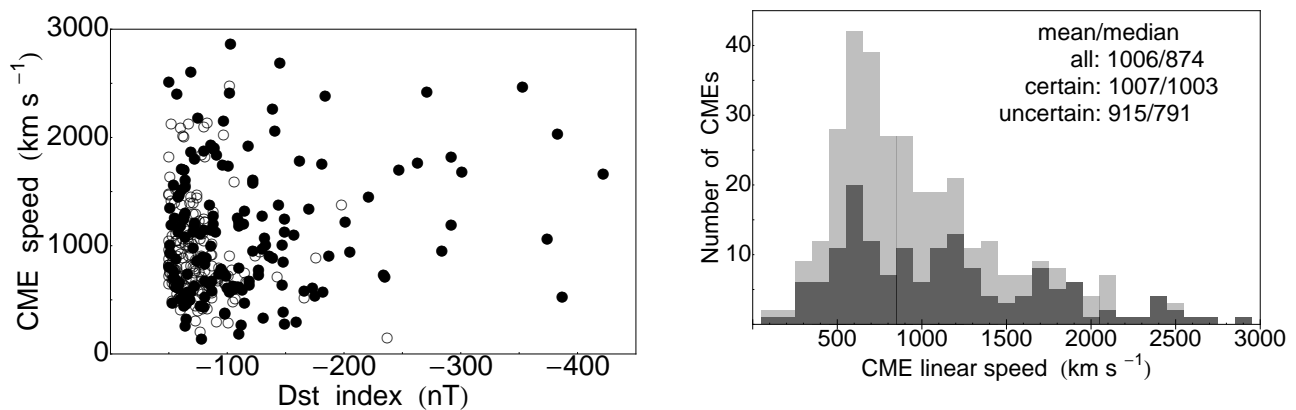


**Figure 4.** Scatter plots between the Dst index (nT) and the CME linear speed (on the left) and the CMEs' speed distribution (on the right, bin width of 100 km s<sup>-1</sup>). Empty circles and light gray color denote uncertain events, whereas filled circles and dark color the certain events.

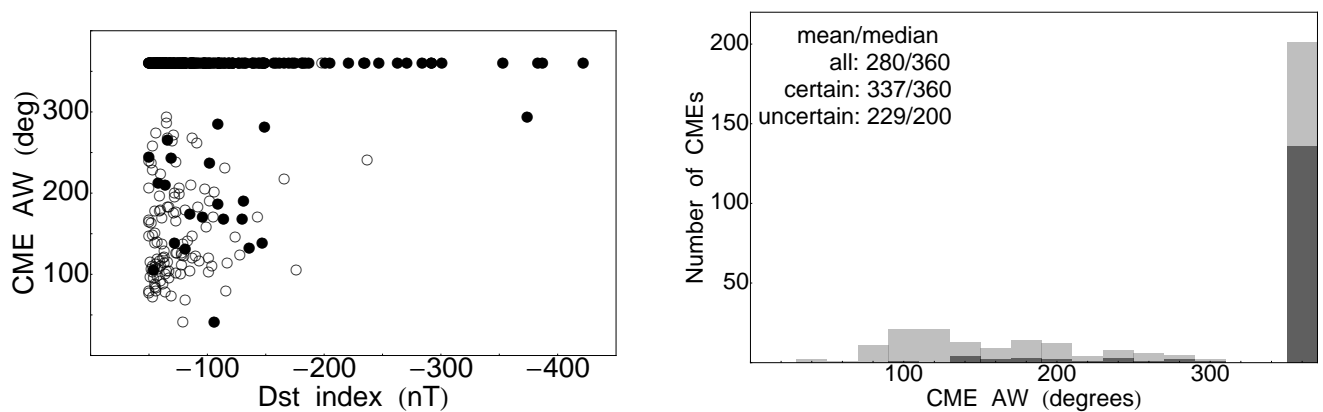


**Figure 5.** Scatter plots between the Dst index (nT) and the CME AW (on the left) and the CME AW distribution (on the right, bin width of 20 degrees). Plotting style as in Figure 4.

The remaining phenomena (SF class and energetic particle flux) covered a range of several orders of magnitudes. This is why the scatter plots are given in log<sub>10</sub>–log<sub>10</sub> form; see Figures 6–8 (left). There was no correlation between the SF class or particle intensities with the Dst index, and the uncertainty was very large, due to the relatively small sample size. The Pearson correlations were calculated between the log<sub>10</sub> values, and the results for the SFs are: certain:  $0.17 \pm 0.08$ , uncertain:  $0.09 \pm 0.10$ , all:  $0.25 \pm 0.06$ . Similarly, for the SEPs, we obtained the following: certain:  $0.15 \pm 0.14$ , uncertain:  $-0.16 \pm 0.20$ , all:  $0.18 \pm 0.12$ , whereas for the SEEs we had: certain:  $0.14 \pm 0.12$ , uncertain:  $0.02 \pm 0.17$ , all:  $0.22 \pm 0.10$ . The sample size is given in Table 1.

All histograms (on the right) are given in binned format, as denoted by the x-label. Overall, the certain sample tended to have the largest mean/median values, followed by the entire sample, and the smallest values were for the uncertain GS-associated SFs, SEPs, and SEEs. The exact mean/median values in SC23+24 are given in the plots.

In the histogram for the SFs, the bins for a given class, e.g., X, were significantly smaller than those of the C- and M-class, the latter two groups being also the most-abundant ones. Also, the number of events denoted by  $6 \div 9$  was always less than the sample denoted by  $1 \div 5$ , independent of the SF class. The mean/median values of the SF class for the certain and all GS-associated SFs were in the lower M-class range, whereas for the uncertain ones, they decreased to the C-class values. Furthermore, we calculated the mean/median value for the helio-locations of the entire sample of GS-associated SFs (no plots are shown) and obtained S01/S06 for the helio-latitude and W04/W05 for the helio-longitude.

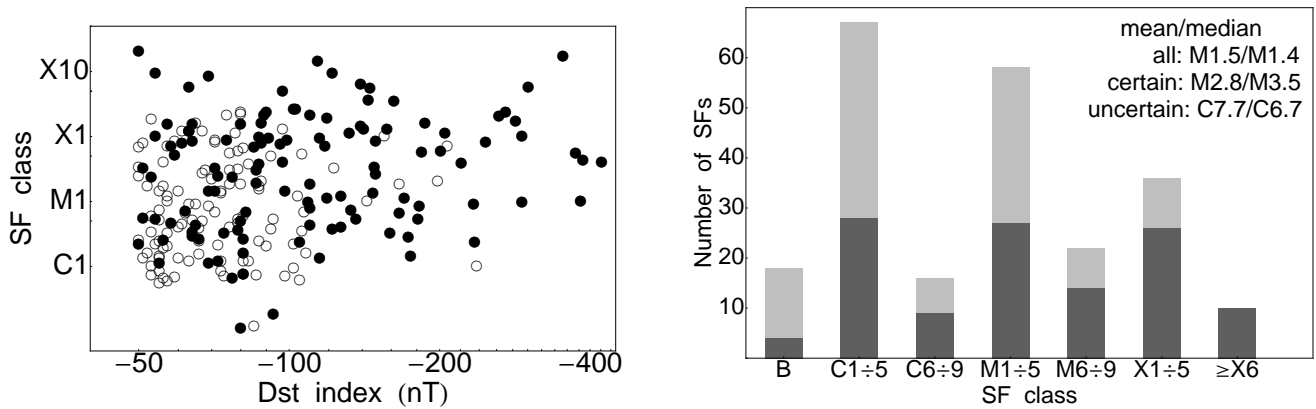


Figure 6. Scatter plots between the Dst index (nT) and the SF class (on the left) and the SF class distribution (on the right). Plotting style as in Figure 4.

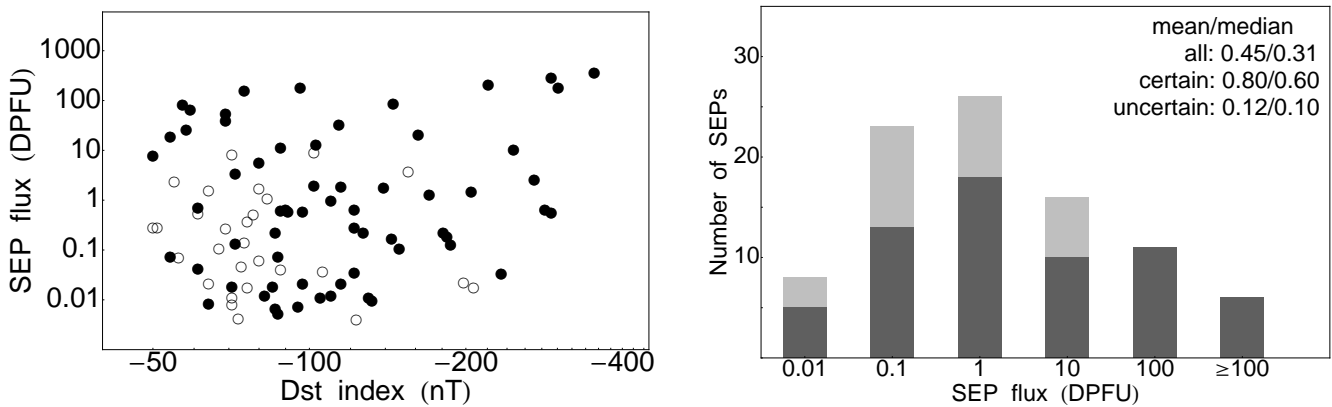


Figure 7. Scatter plots between the Dst index (nT) and the SEP flux (on the left) and the SEP flux distribution (on the right). Plotting style as in Figure 4.

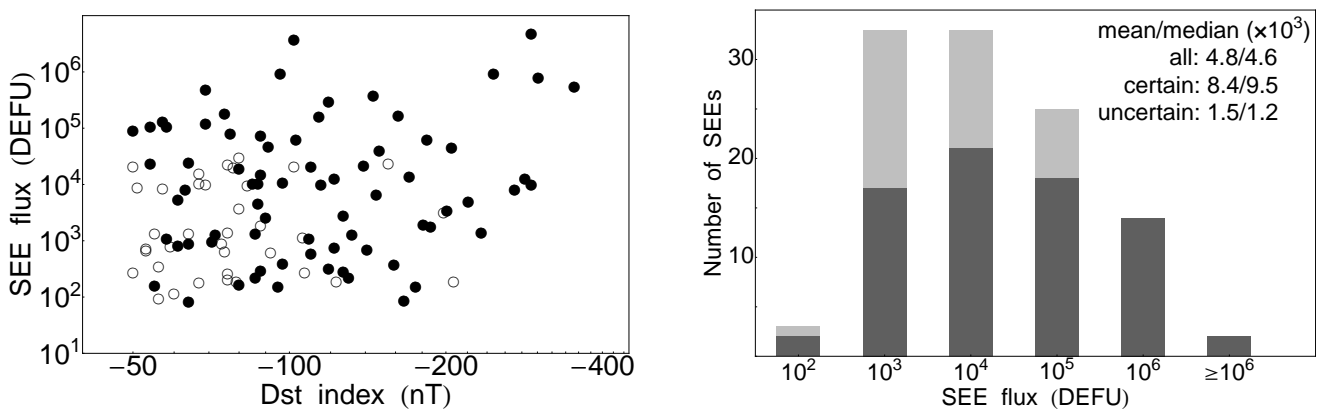


Figure 8. Scatter plots between the Dst index (nT) and the SEE flux (on the left) and the SEE flux distribution (on the right). Plotting style as in Figure 4.

Concerning the particle distributions in Figures 7 and 8, the peak of the distribution was shifted towards the middle, where there were also mean/median values for the certain and also for the entire sample. For completeness, the mean/median values were calculated in the three time periods (Table 1); however, they reflect the weight of the largest bins of the distributions.

#### 4. Discussion

When comparing our results with previously published results of GSs over the same time periods by [32], we noted there were fewer reported events, namely 179 in SC23 and 85 in SC24 (no catalog supplied). Even after eliminating our uncertain GS identification (leading to 331 in SC23 and 166 in SC24), the differences were considerable. The cause of such discrepancies could be due to the different selection criteria applied in either case. According to the results by [32], there was a 47% drop in the geomagnetic activity in SC24 compared to the previous one, which is similar to the one obtained by us of 51% (for the entire GS sample and, similarly, for the certain GSs only). This is one of the studies that explored the relationship between GSs and IP parameters over the same two SCs. The obtained trends by [32] (see their Figures 7 and 8) between the GS indices with the product between solar wind speed and  $B_z$  is reminiscent of the overall trends between the Dst index with ICME and IP shock speeds obtained in our work (Figures 2 and 3).

Another statistical work over SC23 and 24 [35] that presented the occurrence rates between the GSs and the different solar origin phenomena, however, focused on major GSs with  $Dst \leq -100$  nT. Apart from the occurrence rate for the IP shocks (33%, 179/546), which was not considered there, we could still compare the results on GS-associated phenomena. Below, we compare, from one side, the upper limits of the occurrence rates as obtained in our study (with a sample size of 546) and, on the other, the corresponding values in our previous work [35] (with a sample size of 111), namely:

- GSs–ICMEs: 42% (228/546) vs. 85% (94/111);
- GSs–CMEs: 60% (330/546) vs. 72% (80/111);
- GSs–SFs: 42% (227/546) vs. 55% (61/111);
- GSs–SEPs: 16% (90/546) vs. 34% (38/111);
- GSs–SEEs: 20% (110/546) vs. 30% (33/111).

The values obtained in this study (based on a larger sample with numerous weaker GSs) were all smaller. This can be explained by the fact that larger eruptions manifest overall as stronger solar and IP phenomena. Furthermore, we investigated their correlation trends as depicted in the scatter plots and quantified them in terms of the Pearson correlation coefficients. We focused on the results only over SC23+24, and the results in this study were again predominantly lower (but, mostly, not statistically significant) compared to those reported previously by [35], namely:

- Dst–ICME speed:  $0.45 \pm 0.07$  (228) vs.  $0.62$  (94);
- Dst–CME speed:  $0.17 \pm 0.07$  (330) vs.  $0.30$  (80);
- Dst–CME AW:  $0.22 \pm 0.03$  (330) vs.  $0.26$  (80);
- Dst–SF class:  $0.25 \pm 0.06$  (227) vs.  $0.19$  (61);
- Dst–SEP flux:  $0.18 \pm 0.12$  (90) vs.  $0.35$  (38);
- Dst–SEE flux:  $0.22 \pm 0.10$  (110) vs.  $0.27$  (33).

When considering the mean/median values, both studies revealed only marginal differences for the CME speed, but overall, smaller values for the solar parameters. The latter was particularly pronounced in the case of SEE flux, which was two orders of magnitude lower, whereas the SF class and SEP flux were lower by one order of magnitude.

The applicability of statistical results reached an upper limit especially when the sample contained a large amount of scatter and a physical relationship can be easily lost. Moreover, the parameters used for the correlations are often subject to limitations or errors. A greater effort needs to be devoted to the association procedure itself in order to develop procedures for improving its accuracy. A reliable identification of GS precursors would be of use for the development of novel schemes and the improvement of existing forecasting schemes.

Our motivation for the inclusion of GS-related SFs was grounded in the improved understanding of the overall complexity and magnetic environment of the underlying active region that gives rise to the pair SF–CME. The structure and orientation of ICMEs based on the magnetic footprints of their CME counterparts and subsequent IP propagation/rotation/deflection are still subjects of ongoing research [46]. The electromagnetic

emission is also the first signal to be observed after a solar activity event, and its GS precursor potential deserves further examination.

Chronologically, the second space weather phenomena to arrive are the fluxes of electrons, followed by the protons. They possess a latent space weather risk due to their radiation hazards for equipment and humans. Since the charged particles follow a magnetic path, they may well be deflected in the IP space due to magnetic irregularities (in plasma structures), and their forecasting potential is still uncertain. The simultaneous impact of SEP and SEE fluxes from follow-up events to an ongoing GS also awaits a large-scale investigation, although a few single-case studies have been attempted [35]. For example in our earlier analyses [47], low-energy protons tended to be over-represented at minor-to-moderate GSs with  $|Dst| \lesssim 150$  nT, compared to major GSs with  $|Dst| \gtrsim 150$  nT, despite the larger scatter of the distribution. In summary, with this extended study, we confirmed previous studies on the correlations between GSs and the IP/solar origin of GSs [32,35].

## 5. Conclusions

This work offers a consistent list of 546 GSs with Dst index  $\leq -50$  nT in SC23 and 24. ICMEs and IP shock waves preceding the GSs were identified as their most-probable IP origin, whereas the solar origin was based on (fast, halo) CMEs, 3 to 5 days prior to the GSs. Despite the large fraction of uncertain CME (and their secondary) associations, our results were consistent with previous research on the correlations with IP phenomena and with the relationships between solar phenomena and larger GSs.

The focus in this study was set on selected IP and solar phenomena. The GS strength can be correlated with other available physical quantities related to ICMEs, such as plasma density, components of the measured speed, magnetic and electric fields, or a combination thereof, e.g., see [12,32,35,48] and the references therein. The weak correlation between the Dst index and ICME/IP shock speeds could well be due to the limitation to just one of the physical parameters measured in situ. A comprehensive investigation over a large GS sample and using the complete set of physical parameters of ICMEs is still lacking.

A few notable conclusions on the geoeffective IP and solar phenomena, based on the analysis performed here, are listed below:

- Half of the GSs were linked to the arrival of an ICME with IP shocks also present;
- Positive trends in the correlation between the Dst and the speeds of ICMEs and IP shocks were obtained, confirming previous results [32,35];
- There were similar numbers of CMEs (halo and high speed, 330) and ICMEs (228);
- CME to ICME deceleration during its propagation in the solar wind was from 1000/874 to 483/460 km s<sup>-1</sup> in mean/median values;
- No correlation was found between the Dst and the parameters of the solar events (CME speed, CME AW, SF class, or SEP/SEE flux);
- The GS-related solar events originated close to the solar disk center.

The compiled catalog with the values and timings of the GSs and their associated phenomena will be released as open access via the platform <https://catalogs.astro.bas.bg/> (assessed on 26 November 2023) and revised when necessary in the future.

**Author Contributions:** The authors contributed equally to this work. All authors have read and agreed to the published version of the manuscript.

**Funding:** This research was funded by the Bulgarian–Egyptian inter-academy project by the Bulgarian Academy of Sciences IC-EG/08/2022-2024 and the Egyptian Academy of Scientific Research and Technology (ASRT)/NRIAG (ASRT/BAS/2022-2023/10116).

**Institutional Review Board Statement:** Not applicable.

**Informed Consent Statement:** Not applicable.

**Data Availability Statement:** The complete version of the GS catalog will be released at <https://catalogs.astro.bas.bg/>.

**Acknowledgments:** The authors thank the ground-based and space data providers for their free access policy: Kyoto World Data Center—Kyoto, National Aeronautics and Space Administration, and the European Space Agency.

**Conflicts of Interest:** The authors declare no conflict of interest. The funders had no role in the design of the study; in the collection, analyses, or interpretation of the data; in the writing of the manuscript; nor in the decision to publish the results.

### Abbreviations

The following abbreviations are used in this manuscript:

ACE/EPAM	Satellite and instrument for particle detection
AU	Astronomical unit
AW	Angular width
CDAW	Coordinated Data Analyses Workshop
CIR	Co-rotating interaction region
CME	Coronal mass ejection
DEFU	Differential electron flux units
DPFU	Differential proton flux units
GIC	Geomagnetically induced current
GS	Geomagnetic storm
HSS	High-speed solar wind stream
ICME	Interplanetary CME
IMF	Interplanetary magnetic field
IP	Interplanetary
MPA	Measurement position angle
NASA	National Aeronautics and Space Administration
NOAA	National Oceanic and Atmospheric Administration
SC	Solar cycle
SEE	Solar energetic electron
SEP	Solar energetic proton
SF	Solar flare
SOHO/LASCO	Satellite and instrument for CME detection
SSC	Sudden storm commencement
SXR	Soft X-ray
Wind/EPACT	Satellite and instrument for particle detection

### Appendix A. Summary of Occurrence Rates

**Table A1.** Occurrence rates in % of the GS-associated IP and solar phenomena. In parenthesis are shown the fraction of the event type (from Table 1) to the same number of GSs in each of the time periods.

Type	SC23	SC24	SC23+24
ICMEs	44% (159/361)	37% (69/185)	42% (228/546)
IP shocks	35% (127/361)	14% (52/185)	33% (179/546)
CMEs	61% (220/361)	59% (110/185)	60% (330/546)
- certain	32% (114/361)	23% (43/185)	29% (157/546)
SFs	43% (157/361)	39% (70/185)	42% (227/546)
- certain	24% (86/361)	17% (32/185)	22% (118/546)
SEPs	16% (57/361)	19% (33/185)	16% (90/546)
- certain	12% (43/361)	11% (20/185)	12% (63/546)
SEEs	19% (69/361)	22% (41/185)	20% (110/546)
- certain	14% (51/361)	12% (23/185)	14% (74/546)

**Appendix B. Catalog of GSs with Proposed IP and Solar Origin (1996–2019)**

**Table A2.** A catalog of GSs with identified IP and solar origin. The timings of the latter will be given in the online version. The Dst index is in nT; speed in km s<sup>-1</sup>; AW in degrees; rounded SEP flux in DPFU; SEE flux in DEFU. The SF class and location are according to the GOES reports. Abbreviations: u—uncertain; dg—data gap; no—no event found.

yyyy	mm	GS dd	h	Dst	ICME Speed	IP Shock Speed	CME Speed	AW	SF Class	SF Location	SEP Flux	SEE Flux
1996	1	13	11	-90	no	no	499 u	18	no	no	no	no
1996	3	11	4	-60	no	no	u	u	no	no	no	no
1996	3	20	24	-54	no	no	418 u	59	no	no	no	no
1996	3	21	23	-66	no	no	u	u	no	no	no	no
1996	3	24	3	-53	no	no	u	u	no	no	no	no
1996	3	25	2	-60	no	no	u	u	no	no	no	no
1996	4	15	1	-56	no	no	u	u	no	no	no	no
1996	4	17	9	-52	no	no	u	u	no	no	no	no
1996	9	12	9	-54	no	no	u	u	no	no	no	no
1996	9	23	8	-51	no	no	410	27	no	no	no	no
1996	9	27	1	-50	no	no	u	u	no	no	no	no
1996	10	19	17	-52	no	no	u	u	no	no	no	no
1996	10	23	5	-105	no	no	470 u	170	B6.0	no	no	no
1997	1	10	10	-78	450	434	136	360	no	no	no	no
1997	2	10	11	-68	450	618	490	360	no	no	no	no
1997	2	11	10	-60	no	no	u	u	no	no	no	no
1997	2	17	9	-54	no	no	u	u	no	no	no	no
1997	2	27	24	-86	no	543	905 u	209	B7.2	no	no	no
1997	3	28	24	-63	no	no	u	u	no	no	no	no
1997	4	11	5	-82	460	337	878	360	C6.8	S30E19	0.0118	no
1997	4	17	6	-77	no	389	dg	dg	no	no	no	no
1997	4	22	1	-107	360	no	u	u	no	no	no	no
1997	5	2	1	-64	no	361	255 u	360	no	no	no	no
1997	5	15	13	-115	450	443	464 u	360	C1.3	no	0.0202	no
1997	5	27	5	-73	340	303	296 u	165	M1.3	N05W12	0.004	no
1997	6	9	4	-84	380	no	u	u	no	no	no	no
1997	9	3	23	-98	410	368	371	360	M1.4	N30E17	no	no
1997	9	18	6	-56	no	no	u	u	no	no	no	no
1997	10	1	16	-98	450	no	359	360	no	no	no	no
1997	10	10	20	-65	430	471	506	103	no	no	no	no
1997	10	11	4	-130	400	no	1271	167	no	no	0.0108	213
1997	10	25	3	-64	no	no	523	360	C3.3	N16E07	no	79
1997	10	27	23	-60	500	no	503	360	no	no	no	no
1997	11	7	5	-110	400	no	785	360	X2.1	S14W33	0.9518	19,795
1997	11	10	3	-54	no	no	1556	360	X9.4	S18W63	18.13	102,017
1997	11	23	7	-108	510	377	611 u	360	C1.6	no	no	no
1997	12	11	11	-60	350	375	397 u	223	no	no	no	no
1997	12	30	20	-77	370	386	197 u	360	no	no	no	no
1998	1	7	5	-77	400	406	438	360	B6.4	N24W42	no	no
1998	1	30	12	-55	380	no	693	360	C1.1	N21E25	no	no
1998	2	18	1	-100	400	no	u	u	no	no	no	no
1998	2	18	20	-51	440	451	u	u	no	no	no	no
1998	2	20	1	-50	no	no	u	u	no	no	no	no
1998	3	10	21	-116	no	no	659 u	79	no	no	no	no
1998	3	21	16	-85	no	no	636	174	no	no	no	no
1998	3	25	17	-56	400	no	u	u	no	no	no	no
1998	3	29	20	-54	no	no	761	104	C5.3	no	no	no

Table A2. Cont.

yyyy	mm	GS dd	h	Dst	ICME Speed	IP Shock Speed	CME Speed	AW	SF Class	SF Location	SEP Flux	SEE Flux
1998	4	24	8	−69	no	402	1863	243	M1.4	u	37.6	461,152
1998	4	26	18	−63	no	no	1691	360	X1.2	S17E102	no	no
1998	5	2	18	−85	520	631	1374	360	M6.8	S18E20	0.0173	9955
1998	5	4	6	−205	550	474	938	360	X1.1	S15W15	1.423	43,760
1998	6	6	22	−50	no	no	818	147	no	no	no	no
1998	6	14	11	−55	340	273	1223 u	177	M1.4	no	no	no
1998	6	26	5	−101	470	no	278 u	119	no	no	no	u
1998	7	16	17	−58	no	no	dg	dg	no	no	no	no
1998	8	6	12	−138	360	475	dg	dg	no	no	no	no
1998	8	7	6	−108	450	no	dg	dg	no	no	no	no
1998	8	20	21	−67	320	321	dg	dg	no	no	no	no
1998	8	27	10	−155	650	708	dg	dg	X1.0	no	3.609	22,947
1998	9	1	17	−55	no	no	dg	dg	no	no	no	no
1998	9	18	14	−51	no	no	dg	dg	no	no	no	no
1998	9	25	10	−207	640	768	dg	dg	M7.1	N18E09	0.0167	182
1998	10	1	2	−58	no	no	dg	dg	no	no	no	no
1998	10	2	22	−56	no	660	dg	dg	no	no	no	no
1998	10	7	23	−70	no	no	dg	dg	no	no	no	no
1998	10	19	16	−112	390	no	262	360	no	no	no	no
1998	10	20 u	22	−71	no	no	u	u	no	no	no	no
1998	10	22 u	19	−53	520	no	u	u	no	no	no	no
1998	11	6	9	−61	no	no	661 u	169	C4.4	S25E44	no	no
1998	11	7 u	17	−81	450	no	523	360	C1.6	N11W01	no	no
1998	11	8	7	−149	450	645	1118	360	M8.4	N22W18	no	u
1998	11	9	18	−142	no	no	u	u	no	no	no	no
1998	11	13	22	−131	390	406	325	190	no	no	no	no
1998	12	11	16	−69	no	no	806 u	73	no	no	no	no
1998	12	25	12	−57	no	no	752 u	22	no	no	no	no
1998	12	29	12	−58	400	464	u	u	no	no	no	no
1999	1	14	1	−112	420	413	u	u	no	no	no	no
1999	1	23	23	−52	570	701	dg	dg	no	no	no	no
1999	2	18	10	−123	540	700	dg	dg	M3.2	S23W14	0.0038	180
1999	3	1	1	−94	no	no	u	u	no	no	no	no
1999	3	4	24	−52	no	no	u	u	no	no	no	no
1999	3	7	11	−57	no	no	u	u	no	no	no	no
1999	3	10	9	−81	410	501	u	u	no	no	no	no
1999	3	29	15	−56	no	no	u	u	no	no	no	no
1999	4	17	8	−91	410	456	291 u	261	no	no	no	no
1999	7	31	2	−53	480	no	462	360	M2.3	S15E03	no	no
1999	8	23	1	−66	460	no	736	265	C2.6	N23E27	no	no
1999	9	13	5	−74	no	531	1467 u	125	B7.0	no	no	no
1999	9	16	9	−67	no	544	898 u	182	C4.9	N21E02	no	no
1999	9	22	24	−173	530	466	604	360	C2.8	no	no	no
1999	9	27	19	−64	no	no	1150 u	77	no	no	no	no
1999	9	30	4	−61	no	no	u	u	no	no	no	no
1999	10	10	19	−67	no	no	u	u	no	no	no	no
1999	10	22	7	−237	480	476	144 u	240	C1.0	no	no	no
1999	10	28	18	−66	no	no	1127 u	114	C1.5	u	no	no
1999	11	7	16	−67	no	no	u	u	no	no	no	no
1999	11	8	15	−73	no	no	u	u	no	no	no	no
1999	11	11	7	−55	no	no	631 u	87	C5.0	u	no	no
1999	11	13	9	−69	450	no	dg	dg	no	no	no	no
1999	11	13	23	−106	440	466	dg	dg	no	no	no	no
1999	11	16	17	−79	no	no	1104 u	41	C4.6	S12E44	no	no

Table A2. Cont.

yyyy	mm	GS dd	h	Dst	ICME Speed	IP Shock Speed	CME Speed	AW	SF Class	SF Location	SEP Flux	SEE Flux
1999	11	24	10	−50	no	no	dg	dg	no	no	no	no
1999	12	13	10	−85	440	553	dg	dg	no	no	no	no
1999	12	31	24	−50	no	no	u	u	no	no	no	no
2000	1	11	22	−81	no	no	1813 u	67	C5.8	N23W42	no	no
2000	1	23	1	−97	380	no	739	360	M3.9	S19E11	0.0201	381
2000	2	12	12	−133	540	638	1003	360	C7.3	N31E04	no	no
2000	3	31	12	−60	420	no	1177	360	u	u	u	u
2000	4	5	2	−63	no	no	532 u	113	no	no	no	no
2000	4	7	1	−292	560	642	1188	360	C9.7	N16W66	0.5441	9431
2000	4	16	12	−79	no	no	409 u	360	M3.1	S14W01	no	no
2000	4	24	15	−61	500	no	u	u	no	no	no	no
2000	5	17	6	−92	550	no	666 u	182	C3.7	S22E65	no	no
2000	5	24	9	−147	530	656	629	138	no	no	no	no
2000	5	29	21	−54	no	no	u	u	no	no	no	no
2000	6	8	20	−90	610	no	1119	360	X2.3	N20E18	0.6162	2432
2000	6	26	18	−76	520	no	847 u	198	M3.0	N26W72	0.017	21,306
2000	7	16	1	−301	740	no	1674	360	X5.7	N22W07	174.3	750,613
2000	7	20	10	−93	530	638	788 u	116	C5.3	N13E30	no	no
2000	7	22	18	−63	no	497	dg	dg	no	no	no	no
2000	7	23	23	−68	360	no	dg	dg	no	no	no	no
2000	7	29	12	−71	440	no	1287 u	271	M8.0	N06W08	no	no
2000	8	11	7	−106	430	380	597	40	no	no	no	no
2000	8	12	10	−235	580	563	702	360	C2.3	N11W11	no	no
2000	8	29	7	−60	no	no	518 u	178	M1.4	S15E67	no	no
2000	9	12	20	−73	no	no	761 u	176	no	no	u	u
2000	9	17	24	−201	600	no	1215	360	M5.9	N14E07	no	3300
2000	9	19	15	−77	no	no	1056 u	100	no	no	no	no
2000	9	26	3	−55	no	no	u	u	no	no	no	no
2000	9	30	15	−76	no	454	587 u	360	M1.8	N09W18	no	250
2000	10	3	13	−79	no	462	820 u	136	C5.2	N17W52	no	181
2000	10	4	21	−143	400	no	703 u	170	M1.0	S22E36	no	no
2000	10	5	8	−175	no	538	525	360	C1.4	S09E07	no	149
2000	10	5	14	−182	450	no	569	360	C8.4	no	no	u
2000	10	13	6	−71	no	526	798 u	175	C6.7	N01W14	0.0075	no
2000	10	14	15	−107	400	no	506 u	360	u	u	no	257
2000	10	23	8	−53	no	no	u	u	no	no	no	no
2000	10	29	4	−127	380	390	770	360	C4.0	N06W60	0.2115	2665
2000	11	4	10	−50	no	429	801	360	C2.2	S17E39	no	no
2000	11	6	22	−159	510	611	291	360	C3.2	N02W02	no	357
2000	11	10	13	−96	no	925	1738	170	M7.4	N10W77	173.2	888,533
2000	11	27	2	−80	540	524	1245 u	360	X2.3	N22W07	1.643	29,353
2000	11	29	14	−119	540	604	671	360	X1.9	N20W23	no	28,8203
2000	12	23	5	−62	320	314	510	360	C7.0	N15S01	no	no
2001	1	24	19	−61	400	615	1507	360	M7.7	S07S46	0.0399	793
2001	2	13	22	−50	no	651	956 u	360	no?	N37W03	no	no
2001	3	5	3	−73	440	no	631 u	237	C1.2	S09W27	no	no
2001	3	20	14	−149	360	441	271	281	no	no	no	no
2001	3	23	17	−75	no	382	389 u	360	no	N20W0	no	no
2001	3	28	16	−87	610	552	906 u	360	M1.7	N15E22	no	u
2001	3	31	9	−387	640	498	519	360	M4.3	S10E30	no	no
2001	3	31	22	−284	600	565	942	360	X1.7	N20E19	0.6266	12,355
2001	4	5	8	−50	650	845	2505	244	X20	no	7.389	87782
2001	4	9	7	−63	740	696	1270	360	X5.6	S21E31	no	u
2001	4	11	24	−271	640	310	2411	360	X2.3	S23W09	2.499	7716
2001	4	13	16	−77	730	no	1103	360	M2.3	S22W27	no	77,982

Table A2. Cont.

yyyy	mm	GS dd	h	Dst	ICME Speed	IP Shock Speed	CME Speed	AW	SF Class	SF Location	SEP Flux	SEE Flux
2001	4	18	7	−114	430	602	1199	167	X14.4	S20W85	31.3	153,434
2001	4	22	16	−102	350	381	2465 u	360	C2.2	S15W90	8.5	19,759
2001	5	10	4	−76	430	no	1223 u	205	C3.9	N25W35	0.3542	1356
2001	6	18	9	−61	no	336	1701	360	no	no	0.6736	5220
2001	8	17	22	−105	500	519	618	360	C2.3	N24W19	0.0107	no
2001	9	13	8	−57	410	449	791 u	360	C3.2	N13E35	no	u
2001	9	23	19	−73	440	no	436 u	360	no	no	no	no
2001	9	26	2	−102	no	851	2402	360	X2.6	S16E23	1.88	3,551,563
2001	9	30	21	−66	560	483	509 u	182	C3.8	S20W27	no	no
2001	10	1	9	−148	490	no	846	360	M3.3	S18W36	no	no
2001	10	2	13	−104	490	no	773 u	109	M1.2	no	no	no
2001	10	3	15	−166	500	no	509 u	216	M1.8	N13E03	no	no
2001	10	9	16	−64	no	382	1537	360	no	no	no	no
2001	10	12	13	−71	560	579	973	360	M1.4	S28E08	no	no
2001	10	19	22	−57	no	no	u	u	no	no	no	no
2001	10	21	22	−187	460	636	901	360	X1.6	N15W29	0.1236	1739
2001	10	28	12	−157	360	589	1092	360	X1.3	S16W21	no	no
2001	11	1	11	−106	330	395	592 u	200	C3.4	no	no	no
2001	11	6	7	−292	600	no	1810	360	X1.0	N06W18	277.3	4,512,846
2001	11	24	17	−221	720	804	1443	360	M3.8	S25W67	196.7	4715
2001	12	21	23	−67	no	552	1025 u	103	no	no	no	170
2001	12	24	11	−55	no	306	769 u	108	C2.4	no	no	no
2001	12	30	6	−58	400	669	1446	212	M7.1	N08W54	24.47	103,570
2002	1	11	7	−72	no	no	1794	360	no	no	no	no
2002	2	2	10	−86	no	no	1136	360	no	no	0.2095	1267
2002	2	5	21	−82	no	no	u	u	no	no	no	no
2002	3	1	2	−71	390	no	u	u	no	no	no	no
2002	3	24	10	−100	450	517	603	360	no	no	no	no
2002	4	18	8	−127	480	517	720	360	M1.2	S15W01	no	267
2002	4	19 u	19	−126	no	768	u	u	no	no	no	no
2002	4	20	9	−149	500	no	1240	360	M2.6	S14W34	0.1024	38,361
2002	4	23	16	−57	no	644	2393	360	X1.5	S14W84	79.07	127,221
2002	5	11	20	−110	430	483	614	360	C4.2	S12W07	no	no
2002	5	14	21	−63	no	no	1154 u	120	C1.2	S18W43	no	no
2002	5	19	7	−58	no	545	600	360	C4.5	S23E15	no	no
2002	5	23	18	−109	590	737	1246	186	C9.7	N17E36	no	1032
2002	5	27	9	−64	no	no	1557 u	360	C5.0	S30W34	1.517	no
2002	8	1	14	−51	no	no	u	u	no	no	no	no
2002	8	2	6	−102	460	496	562	236	no	no	no	no
2002	8	02 u	23	−69	no	no	u	u	no	no	no	no
2002	8	4	6	−58	no	no	u	u	no	no	no	no
2002	8	19	8	−53	no	672	u	u	no	no	no	no
2002	8	20	1	−71	no	535	u	u	no	no	no	no
2002	8	21	7	−106	460	no	1585 u	360	M5.2	S14E20	0.0349	1082
2002	9	4	6	−109	no	340	u	u	no	no	no	no
2002	9	8	1	−181	470	897	1748	360	C5.2	N09E28	0.2118	1886
2002	9	10	1	−69	no	no	909 u	360	no	no	no	no
2002	9	11	23	−90	no	no	u	u	no	no	no	no
2002	10	1	21	−176	390	331	881 u	104	no	no	no	no
2002	10	2 u	5	−158	no	no	u	u	no	no	no	no
2002	10	4	9	−146	430	no	u	u	no	no	no	no
2002	10	5	16	−102	no	no	903 u	190	B9.2	S18E20	no	no
2002	10	7	8	−115	no	no	743 u	230	no	no	no	no
2002	10	8 u	5	−108	no	no	u	u	no	no	no	no
2002	10	14	14	−100	no	no	u	u	no	no	no	no
2002	10	15 u	19	−70	no	no	1009 u	264	M2.2	S08E66	no	u

Table A2. Cont.

yyyy	mm	GS dd	h	Dst	ICME Speed	IP Shock Speed	CME Speed	AW	SF Class	SF Location	SEP Flux	SEE Flux
2002	10	16	21	−63	no	no	1694 u	360	no	no	no	no
2002	10	24	21	−98	no	no	640 u	360	no	no	no	no
2002	10	25 u	2	−91	no	no	u	u	no	no	no	no
2002	10	26 u	20	−62	no	no	1052 u	119	C6.6	S04W62	no	no
2002	10	27 u	16	−65	no	no	689 u	286	no	no	no	no
2002	10	28 u	5	−63	no	no	629 u	360	no	no	no	no
2002	10	30 u	19	−52	no	no	2115 u	360	no	no	no	no
2002	11	3	4	−74	no	no	u	u	no	no	no	no
2002	11	18	23	−52	380	no	1185	360	no	no	no	no
2002	11	20	21	−87	no	392	1008 u	119	C2.4	no	no	no
2002	11	21	11	−128	no	no	938 u	123	no	no	no	no
2002	11	27	7	−64	no	no	1077	360	no	no	no	851
2002	12	19	21	−72	no	no	u	u	no	no	no	no
2002	12	20 u	6	−64	no	no	u	u	no	no	no	no
2002	12	21 u	4	−75	440	no	u	u	no	no	no	no
2002	12	23	12	−67	no	no	1092 u	360	M2.7	N15W09	0.1002	9777
2002	12	27	5 17	−68	no	no	u	u	no	no	no	no
2003	1	30	1	−66	no	no	1053 u	267	C2.4	S17W23	no	no
2003	2	2	18	−72	510	no	620	138	no	no	no	no
2003	2	4	10	−74	no	no	u	u	no	no	no	no
2003	2	4 u	24	−54	no	no	u	u	no	no	no	no
2003	2	27	22	−66	no	no	u	u	no	no	no	no
2003	3	4	1	−67	no	no	u	u	no	no	no	no
2003	3	16	22	−60	no	no	1021 u	91	C1.3	S12E09	dg	no
2003	3	20	20	−64	650	no	1601	209	X1.5	S15W46	0.008	23,895
2003	3	27	18	−56	no	no	1505 u	82	C1.9	S17E77	no	no
2003	3	29 u	7	−63	no	no	u	u	no	no	no	no
2003	3	29 u	21	−70	no	no	u	u	no	no	no	no
2003	3	31 u	16	−78	no	no	664 u	111	no	no	no	no
2003	4	2	23	−53	no	no	u	u	no	no	no	no
2003	4	4	24	−62	no	no	885 u	87	no	no	no	no
2003	4	25	23	−53	no	no	899 u	148	B7.2	no	no	no
2003	4	30	3	−67	no	no	991 u	95	no	no	no	no
2003	5	10	9	−84	680	no	u	u	no	no	no	no
2003	5	22	3	−73	no	no	866 u	101	B8.3	u	no	no
2003	5	30	1	−144	600	907	1366	360	X3.6	S07W20	0.1636	no
2003	5	31	6	−63	680	no	1237	360	X1.2	S06W37	no	7886
2003	6	2	9	−91	no	no	1835	360	M9.3	S07W65	0.5543	45,772
2003	6	8	23	−50	no	no	1458 u	239	no	no	no	no
2003	6	16 u	17	−59	no	no	u	u	no	no	no	no
2003	6	16	23	−68	510	no	u	u	no	no	no	no
2003	6	17	9	−81	no	no	1215 u	179	no	no	no	no
2003	6	18	10	−141	480	479	2053	360	X1.3	S07E80	no	656
2003	6	21	10	−50	no	no	1813 u	360	M6.8	S08E58	0.2634	20,103
2003	6	24	14	−55	no	no	u	u	no	no	no	no
2003	7	11	11	−55	no	no	u	u	no	no	no	no
2003	7	12	6	−105	no	no	u	u	no	no	no	no
2003	7	16	14	−90	no	no	u	u	no	no	no	no
2003	7	19	1	−50	no	no	u	u	no	no	no	no
2003	7	27	8	−57	no	no	u	u	no	no	no	no
2003	8	6	7	−60	440	no	699 u	360	no	no	no	no
2003	8	7	22	−61	no	no	u	u	no	no	no	no
2003	8	18	16	−148	450	no	378	360	no	no	no	no
2003	8	21	24	−68	no	no	u	u	no	no	no	no
2003	9	17	24	−65	no	no	u	u	no	no	no	no
2003	9	24	8	−59	no	no	646	360	no	no	no	no

Table A2. Cont.

yyyy	mm	GS dd	h	Dst	ICME Speed	IP Shock Speed	CME Speed	AW	SF Class	SF Location	SEP Flux	SEE Flux
2003	10	14	23	−85	no	no	u	u	no	no	no	no
2003	10	17	7	−53	no	no	u	u	no	no	no	no
2003	10	20 u	22	−57	no	no	627 u	360	no	no	no	no
2003	10	22 u	7	−61	520	no	u	u	no	no	no	no
2003	10	27	5	−52	470	no	1406 u	236	M1.7	S04E13	u	u
2003	10	30	1	−353	1300	no	2459	360	X17.2	S16E68	353.2	530,064
2003	10	30	23	−383	800	no	2029	360	M1.0	S15W02	no	no
2003	11	4	11	−69	no	759	2598	360	X8.3	S14W56	50.99	116,852
2003	11	11	14	−62	no	no	2008 u	360	no	no	no	no
2003	11	20	21	−422	580	666	1660	360	M3.9	N00E18	u	u
2003	11	22	23	−87	no	no	669	360	M9.6	N01W08	0.0694	9787
2003	12	6	5	−55	no	no	1393 u	150	C7.2	S19W91	2.225	1281
2003	12	8 u	22	−54	no	no	676 u	95	C2.2	S17W38	no	no
2003	12	10 u	20	−51	no	no	u	u	no	no	no	no
2004	1	7	14	−50	no	no	1469 u	166	C2.5	no	no	no
2004	1	15	17	−50	no	no	u	u	no	no	no	no
2004	1	22	14	−130	560	no	965	360	no	no	no	no
2004	1	25 u	4	−81	490	no	762 u	360	C1.2	S19E29	no	no
2004	1	27 u	2	−62	no	no	u	u	no	no	no	no
2004	2	11	18	−93	no	no	u	u	no	no	no	no
2004	3	9	24	−72	no	no	u	u	no	no	no	no
2004	3	11	24	−63	no	no	u	u	no	no	no	no
2004	4	4	1	−117	440	no	652 u	113	no	no	no	no
2004	4	5	20	−62	no	no	u	u	no	no	no	no
2004	7	17	3	−76	no	no	747 u	360	M5.4	N12W52	no	198
2004	7	23	3	−99	560	454	710	360	M8.6	N10E35	no	no
2004	7	25	17	−136	560	561	899	132	C5.3	N04E10	no	u
2004	7	27	14	−170	870	1086	1333	360	M1.1	N08E33	1.245	13,269
2004	8	9	22	−51	no	no	1004	360	no	no	no	no
2004	8	30	23	−129	390	483	u	u	no	no	no	no
2004	11	8	7	−374	630	742	1055	293	M5.4	N08E18	no	no
2004	11	10	11	−263	640	813	1759	360	X2.0	N09W17	u	no
2004	11	25	8	−53	no	no	649 u	102	no	no	no	no
2004	11	28	7	−50	no	no	u	u	no	no	no	no
2004	12	13	3	−56	400	no	611	360	C2.5	N01W07	no	no
2005	1	8	3	−93	460	560	735	360	B1.8	S15E15	no	no
2005	1	12	11	−50	no	no	870 u	164	M2.4	S09E69	no	no
2005	1	17	4	−65	520	539	455	360	C4.2	S06E15	no	no
2005	1	18	9	−103	no	no	2861	360	X2.6	N14W08	12.71	59,664
2005	1	19 u	11	−80	800	no	2094 u	360	X2.2	N13W19	u	u
2005	1	22	6	−97	no	no	2020 u	360	X1.3	N15W51	no	no
2005	2	7	22	−57	no	no	711 u	139	no	no	no	no
2005	2	18	3	−80	410	no	1135	360	C4.9	S03W23	no	162
2005	3	7	1	−54	no	no	u	u	no	no	no	no
2005	4	5	5	−70	no	472	u	u	no	no	no	no
2005	4	12	6	−62	no	no	u	u	no	no	no	no
2005	5	8	3	−82	no	438	u	u	no	no	no	no
2005	5	8	19	−110	no	476	1180	360	C7.8	N04W67	no	no
2005	5	15	9	−247	630	858	1689	360	M8.0	N12E11	9.876	879,497
2005	5	20	9	−83	430	no	405 u	140	C1.2	N15W27	no	u
2005	5	30	14	−113	460	u	586	360	no	no	no	no
2005	6	13	1	−106	480	no	u	u	no	no	no	no
2005	6	23	11	−85	no	no	614 u	103	B1.2	S13W51	no	no

Table A2. Cont.

yyyy	mm	GS dd	h	Dst	ICME Speed	IP Shock Speed	CME Speed	AW	SF Class	SF Location	SEP Flux	SEE Flux
2005	7	9	21	−55	no	no	772 u	360	C1.3	S08E34	no	no
2005	7	10	21	−92	430	533	683 u	360	M4.9	N09E03	no	579
2005	7	18	7	−67	420	378	2115 u	360	X1.2	N11W90	no	14,743
2005	8	24	12	−184	660	536	2378	360	M5.6	S13W65	0.1792	59,728
2005	8	31	20	−122	no	no	1600	360	no	no	0.0328	714
2005	9	4	10	−71	pd	no	1384 u	360	no	no	no	no
2005	9	10 u	23	−73	no	544	1291 u	126	M1.4	S12E88	no	no
2005	9	11	11	−139	900	1147	2257	360	X6.2	S10E58	no	no
2005	9	12 u	22	−89	750	1048	1893	360	X2.1	S13E47	no	no
2005	9	13 u	13	−86	630	no	1922	360	M3.0	S16E39	no	no
2005	9	15	17	−80	680	661	1866	360	X1.5	S09E10	5.515	18,409
2005	10	8	8	−50	no	no	u	u	no	no	no	no
2005	10	31	21	−74	360	no	u	u	no	no	no	no
2005	12	11	19	−55	480	no	673 u	360	B5.5	N15E14	no	no
2006	1	26	4	−51	no	no	u	u	no	no	no	no
2006	3	7	2	−52	no	no	u	u	no	no	no	no
2006	4	5	16	−79	no	no	u	u	no	no	no	no
2006	4	9	8	−82	no	no	u	u	no	no	no	no
2006	4	14	10	−98	520	no	u	u	no	no	no	no
2006	5	6	22	−53	no	no	487 u	360	C1.0	S17W02	no	no
2006	8	20	2	−79	400	460	888	360	C3.6	S14W13	no	no
2006	9	24	10	−55	no	402	u	u	no	no	no	no
2006	10	1	6	−51	no	356	u	u	no	no	no	no
2006	10	13	23	−55	no	no	u	u	no	no	no	no
2006	10	29	9	−50	no	no	u	u	no	no	no	no
2006	11	10	2	−63	no	360	1994 u	360	C8.8	no	no	no
2006	11	30	14	−74	420	no	u	u	no	no	no	no
2006	12	6	13	−55	no	no	u	u	no	no	no	no
2006	12	15	8	−162	740	1012	1774	360	X3.4	S06W23	20.17	158,754
2007	3	24	9	−72	no	no	u	u	no	no	no	no
2007	4	1	9	−63	no	no	u	u	no	no	no	no
2007	5	23	14	−58	no	no	958 u	106	no	no	no	u
2007	10	25	22	−53	no	433	u	u	no	no	no	no
2007	11	20	21	−59	460	442	u	u	no	no	no	no
2008	2	28	8	−52	no	no	u	u	no	no	no	no
2008	3	9	6	−86	no	no	u	u	no	no	no	no
2008	3	27	22	−56	no	no	1103 u	112	M1.7	S13E78	no	no
2008	9	4	5	−51	no	no	u	u	no	no	no	no
2008	10	11	12	−54	no	no	u	u	no	no	no	no
2009	7	22	7	−83	330	337	u	u	no	no	no	no
2010	2	15	24	−59	no	336	509 u	360	M8.3	N26E11	no	744
2010	4	6	15	−81	640	no	668	360	B7.4	S25W00	no	no
2010	4	12	2	−67	410	465	u	u	no	no	no	no
2010	5	2	19	−71	no	no	u	u	no	no	no	no
2010	5	29	13	−80	360	no	427	360	B1.1	N13W31	no	no
2010	6	4	2	−53	no	no	u	u	no	no	no	no
2010	8	4	2 20	−74	530	537	850	360	C3.2	N20E36	no	no
2010	10	11	20	−75	no	no	u	u	no	no	no	no
2011	2	4	22	−63	430	no	437	360	no	no	no	no
2011	3	1	15	−88	no	no	u	u	no	no	no	no
2011	3	11	6	−83	no	no	2125 u	360	M3.7	N31W53	1.012	9316
2011	4	6	19	−60	no	no	2081 u	109	no	no	no	no
2011	5	28	12	−80	510	no	657 u	122	no	no	no	no
2011	7	5	1	−59	nd	no	511 u	196	no	no	no	no
2011	8	6	4	−115	no	577	1315	360	M9.3	N19W36	1.79	9625
2011	9	10	5	−75	470	no	575 u	360	X2.1	N14W18	0.1368	622
2011	9	17	16	−72	430	506	746 u	199	no	no	no	no

Table A2. Cont.

yyyy	mm	GS dd	h	Dst	ICME Speed	IP Shock Speed	CME Speed	AW	SF Class	SF Location	SEP Flux	SEE Flux
2011	9	26	24	−118	580	556	1915	360	M7.1	N10E56	no	no
2011	9	28	7	−68	no	no	972 u	360	M3.0	N12E42	no	no
2011	10	25	2	−147	460	no	1005	360	M1.3	N25W77	no	6239
2011	11	1	16	−66	380	334	570	360	no	no	no	no
2012	1	23	6	−71	450	443	1120	360	M3.2	N32E22	0.0173	939
2012	1	25	11	−75	no	736	2175	360	M8.7	N28W21	153.2	170,580
2012	2	15	17	−67	370	no	533 u	360	no	no	no	no
2012	2	19	5	−63	no	no	538 u	360	no	no	no	no
2012	2	27	20	−57	440	no	1039 u	97	B5.9	no	no	no
2012	3	2	2	−54	nd	no	466 u	360	no	no	no	no
2012	3	4	2	−50	no	no	710 u	206	M3.3	N16E83	no	no
2012	3	7	10	−88	no	480	1306 u	360	M2.0	N19E61	0.0384	1801
2012	3	9	9	−145	550	no	2684	360	X5.4	N17E27	82.93	370,966
2012	3	12	17	−64	no	no	1296	360	M8.4	N17W24	no	no
2012	3	15	21	−88	680	no	1884	360	M7.9	N17W66	10.91	70,886
2012	3	28	5	−68	no	no	1390 u	360	no	no	no	no
2012	4	5	8	−64	no	no	u	u	no	no	no	no
2012	4	13	5	−60	no	no	921 u	360	C3.9	N20W65	no	111
2012	4	24	5	−120	370	425	u	u	no	no	no	no
2012	6	12	2	−67	no	no	u	u	no	no	no	no
2012	6	17	14	−86	440	483	987	360	M1.9	S17E06	0.0064	212
2012	7	9	13	−78	410	no	1828 u	360	X1.1	S13W59	0.4885	19,052
2012	7	15	17	−139	490	746	885	360	X1.4	S15W01	1.683	21,061
2012	9	3	11	−69	310	429	1442 u	360	C8.4	S19E42	0.2617	9584
2012	9	5	6	−64	500	482	538	360	C2.9	N03W05	no	no
2012	10	1	5	−122	370	447	947	360	C3.7	N06W34	0.2716	12,151
2012	10	8 u	13	−99	no	465	u	u	no	no	no	no
2012	10	9	9	−109	390	no	612	284	no	no	no	no
2012	10	13	8	−90	490	465	692 u	122	C2.0	S26E86	no	no
2012	11	1	21	−65	340	390	317	360	no	no	no	no
2012	11	14	8	−108	380	no	u	u	no	no	no	no
2013	1	17	24	−52	390	335	798 u	162	no	no	no	no
2013	1	26	23	−51	no	354	u	u	no	no	no	no
2013	3	1	11	−55	no	no	622 u	138	B8.3	S19W05	no	no
2013	3	17	21	−132	520	765	1063	360	X1.1	N11E11	0.009	1247
2013	3	29	17	−59	no	206	663 u	177	B6.8	no	no	no
2013	5	1	19	−72	430	447	u	u	no	no	no	no
2013	5	18	5	−61	no	452	1366 u	360	X1.2	N12E64	0.5234	u
2013	5	19 u	15	−51	no	497	1345	360	M3.2	N12E57	no	no
2013	5	25	7	−59	no	624	1466	360	50	N14W87	61.84	no
2013	5	25 u	20	−56	no	475	u	u	no	no	no	no
2013	6	1	9	−124	no	no	u	u	no	no	no	no
2013	6	7	3	−78	430	no	709 u	123	no	no	no	no
2013	6	29	7	−102	390	no	u	u	no	no	no	no
2013	7	6	19	−87	350	no	807 u	267	M1.5	S11E82	no	no
2013	7	10	22	−56	no	no	u	u	no	no	no	no
2013	7	14	23	−81	430	no	449 u	360	B7.6	N19E14	no	no
2013	8	5	3	−50	no	no	u	u	no	no	no	no
2013	8	27	22	−59	no	no	u	u	no	no	no	no
2013	10	2	8	−72	470	654	1179	360	C1.2	N10W43	3.208	no
2013	10	9	2	−69	480	no	567	360	C1.1	S16W13	no	no
2013	10	30	24	−54	no	337	695	360	X1.0	N04W66	0.0701	22,413
2013	11	7	13	−50	no	no	1040 u	360	no	no	no	259.94
2013	11	9	9	−80	420	428	1033 u	360	M1.8	S11W97	0.0578	3644
2013	11	11	8	−68	nd	no	497 u	360	no	no	no	no
2013	12	8	9	−66	no	329	u	u	no	no	no	no

Table A2. Cont.

yyyy	mm	GS dd	h	Dst	ICME Speed	IP Shock Speed	CME Speed	AW	SF Class	SF Location	SEP Flux	SEE Flux
2014	2	19	9	−119	520	621	634	360	M1.1	S11E01	no	305
2014	2	20	13	−95	490	no	779	360	no	no	0.0071	147
2014	2	22 u	2	−64	n	no	612 u	360	no	no	0.0199	1263
2014	2	23	20	−55	no	no	1252	360	no	no	no	156
2014	2	27	24	−97	no	436	2147	360	X4.9	S12E82	0.566	10,469
2014	3	1	9	−52	no	no	u	u	no	no	no	no
2014	4	12	10	−87	350	no	514 u	360	no	no	no	no
2014	4	30	10	−67	310	no	u	u	no	no	no	no
2014	8	27	19	−79	no	no	551 u	360	M5.9	S07E75	no	no
2014	9	12	24	−88	600	no	1267	360	X1.6	N14E02	0.5808	14,581
2014	10	9	8	−51	no	no	u	u	no	no	no	no
2014	10	28	2	−57	no	no	u	u	no	no	no	no
2014	11	10	18	−65	480	no	795 u	293	X1.6	N15E33	no	no
2014	11	16	8	−59	no	no	710 u	115	no	no	no	no
2014	12	12	17	−53	no	no	1086 u	228	C5.9	S18W89	no	no
2014	12	22	6	−71	380	no	587 u	360	M8.7	S20E09	0.0107	no
2014	12	23 u	23	−57	no	no	1195 u	360	M6.9	S11E15	no	7979
2014	12	24 u	23	−53	no	no	830 u	257	X1.8	S21W24	no	no
2014	12	26 u	2	−57	no	no	669 u	360	M1.0	S14W25	no	no
2015	1	4	22	−78	pd	no	902 u	126	no	no	no	no
2015	1	7	12	−107	450	no	u	u	no	no	no	no
2015	2	2	7	−55	no	no	u	u	no	no	no	no
2015	2	18	1	−69	no	no	u	u	no	no	no	no
2015	2	24	8	−58	no	no	1120	360	no	no	no	1046
2015	3	1	9	−56	no	no	u	u	no	no	no	no
2015	3	2	9	−64	no	no	999 u	360	no	no	no	no
2015	3	17	23	−234	560	536	719	360	C9.1	S22W25	0.0325	1345
2015	4	10	5	−60	no	382	u	u	no	no	no	no
2015	4	11	10	−85	380	no	u	u	no	no	no	no
2015	4	15 u	21	−62	no	no	u	u	no	no	no	no
2015	4	16 u	8	−81	no	371	u	u	no	no	no	no
2015	4	16	24	−88	no	prev	1198	360	no	no	no	284
2015	6	8	9	−67	no	368	u	u	no	no	no	no
2015	6	23	5	−198	610	368	1366 u	360	M2.0	N12E16	0.021	3019
2015	6	25	17	−81	550	748	1209 u	360	M6.5	N12W08	no	no
2015	6	26 u	18	−51	490	no	1627 u	360	M7.9	N09W42	0.2726	8319
2015	7	5	6	−74	no	no	1435 u	360	no	no	0.045	859
2015	7	13	16	−68	490	no	u	u	no	no	no	no
2015	7	23	9	−72	no	no	782 u	194	C2.1	S25W62	u	u
2015	8	16	8	−98	500	477	647 u	204	B7.0	no	no	no
2015	8	19	7	−64	no	no	622 u	X1.0	u	no	no	no
2015	8	23	9	−57	no	no	547 u	360	M1.2	S15E13	no	no
2015	8	26 u	22	−79	no	no	u	u	no	no	no	no
2015	8	27 u	6	−92	no	no	u	u	no	no	no	no
2015	8	27	21	−103	370	no	u	u	no	no	no	no
2015	8	28 u	10	−102	no	no	u	u	no	no	no	no
2015	9	4	7	−50	no	no	u	u	no	no	no	no
2015	9	7	21	−75	no	no	u	u	no	no	no	no
2015	9	9	13	−105	460	no	u	u	no	no	no	no
2015	9	11	15	−87	no	no	556 u	146	no	no	no	no
2015	9	20	16	−81	510	716	823	131	C2.6	S21W10	no	no
2015	10	4	10	−63	no	no	602 u	128	no	no	no	no
2015	10	6	20	−52	no	no	914 u	106	C1.6	S18W66	no	no
2015	10	7	10	−101	no	no	714 u	102	no	no	no	no
2015	10	7	23	−124	no	no	900 u	145	no	no	no	no
2015	10	18	10	−56	no	no	770	79	B6.4	S06E76	no	90

Table A2. Cont.

yyyy	mm	GS dd	h	Dst	ICME Speed	IP Shock Speed	CME Speed	AW	SF Class	SF Location	SEP Flux	SEE Flux
2015	11	3 u	13	−51	no	no	751 u	114	C1.3	N07E30	no	no
2015	11	4	13	−56	640	no	867	360	no	no	no	no
2015	11	7	7	−87	500	no	578	360	M3.7	N09W04	0.005	4425
2015	11	9 u	17	−55	no	no	u	u	no	no	no	no
2015	11	10	14	−56	no	no	1041 u	273	M3.9	S11E41	0.0675	338
2015	12	14	20	−55	no	no	628 u	84	C1.4	S15E52	no	no
2015	12	20	23	−166	400	536	579	360	C6.6	S13W04	no	84
2016	1	1	1	−110	440	no	1212	360	M1.8	S23W11	0.0115	572
2016	1	20	17	−101	370	no	1730	360	no	no	no	no
2016	2	1	9	−53	no	no	684 u	71	C3.3	N09W50	no	689
2016	2	3	3	−57	no	no	901 u	118	C2.0	S20W63	no	no
2016	2	16	20	−65	no	no	719 u	360	C8.9	N09W08	no	no
2016	2	18	1	−62	no	no	u	u	no	no	no	no
2016	3	6	22	−99	pd	no	644 u	158	no	no	no	no
2016	3	15	8	−50	no	398	641 u	79	no	no	no	no
2016	3	16 u	24	−56	no	no	u	u	no	no	no	no
2016	4	2	24	−59	no	no	u	u	no	no	no	no
2016	4	7	22	−61	no	no	u	u	no	no	no	no
2016	4	13	2	−56	no	no	u	u	no	no	no	no
2016	4	14	21	−61	420	no	543 u	136	no	no	no	no
2016	4	16	22	−58	nd	no	u	u	no	no	no	no
2016	5	8	8	−95	no	no	u	u	no	no	no	no
2016	8	3	16	−52	pd	no	u	u	no	no	no	no
2016	8	23	22	−73	no	no	u	u	no	no	no	no
2016	9	1	10	−57	no	no	u	u	no	no	no	no
2016	9	2 u	3	−59	no	no	u	u	no	no	no	no
2016	9	28 u	18	−51	no	no	u	u	no	no	no	no
2016	9	29 u	10	−65	no	no	u	u	no	no	no	no
2016	10	4	10	−50	no	no	818 u	76	no	no	no	no
2016	10	13	18	−110	390	415	179	360	no	no	no	no
2016	10	25	18	−65	no	no	u	u	no	no	no	no
2016	10	29	4	−70	no	no	u	u	no	no	no	no
2016	11	10	18	−60	360	344	u	u	no	no	no	no
2017	3	1	22	−61	no	no	u	u	no	no	no	no
2017	3	27	15	−70	no	no	u	u	no	no	no	no
2017	3	31	7	−51	no	no	u	u	no	no	no	no
2017	4	22	17	−51	no	no	926	360	C5.5	N14E77	no	no
2017	5	28	8	−125	360	373	u	u	no	no	no	no
2017	7	16	16	−72	520	no	1200	360	M2.4	S06W29	0.1284	1248
2017	8	31	12	−51	no	418	u	u	no	no	no	no
2017	9	8	2	−122	220	245	1571	360	X9.3	S08W33	0.604	u
2017	9	8	18	−109	no	no	u	u	no	no	no	no
2017	9	28	7	−56	no	no	u	u	no	no	no	no
2017	10	14	6	−53	no	no	741 u	109	no	no	no	639
2017	11	8	2	−73	no	no	u	u	no	no	no	no
2018	3	18	22	−50	no	no	u	u	no	no	no	no
2018	4	20	10	−66	no	313	u	u	no	no	no	no
2018	5	6	3	−57	no	376	u	u	no	no	no	no
2018	8	26	7	−175	410	no	u	u	no	no	no	no
2018	9	11	11	−60	no	no	u	u	no	no	no	no
2018	10	7	22	−53	no	no	u	u	no	no	no	no
2018	11	5	6	−53	no	no	u	u	no	no	no	no
2019	5	11	22	−51	350	411	745 u	M9.6	u	no	no	no
2019	5	14	8	−65	470	no	u	u	no	no	no	no
2019	8	5	21	−53	no	no	u	u	no	no	no	no
2019	9	1	7	−52	no	no	u	u	no	no	no	no

## References

1. Dungey, J.W. Interplanetary Magnetic Field and the Auroral Zones. *Phys. Rev. Lett.* **1961**, *6*, 47–48. [[CrossRef](#)]
2. Lakhina, G.; Tsurutani, B.; Gonzalez, W.; Alex, S. Humboldt, Alexander Von And Magnetic Storms. In *Encyclopedia of Geomagnetism and Paleomagnetism*; Gubbins, D., Herrero-Bervera, E., Eds.; Springer: Dordrecht, The Netherlands, 2007. [[CrossRef](#)]
3. Gonzalez, W.D.; Joselyn, J.A.; Kamide, Y.; Kroehl, H.W.; Rostoker, G.; Tsurutani, B.T.; Vasyliunas, V.M. What is a geomagnetic storm? *J. Geophys. Res.* **1994**, *99*, 5771–5792. [[CrossRef](#)]
4. Lazzús, J.A.; Salfate, I.; Vega-Jorquera, P. Intense Geomagnetic Storms in The Maximum Phase of Solar Cycle 24 Observed From a Low-Latitude Ground Station. *Geofis. Int.* **2022**, *61*, 267–286. [[CrossRef](#)]
5. Tsurutani, B.T.; Gonzalez, W.D.; Tang, F.; Akasofu, S.I.; Smith, E.J. Origin of interplanetary southward magnetic fields responsible for major magnetic storms near solar maximum (1978–1979). *J. Geophys. Res.* **1988**, *93*, 8519–8531. [[CrossRef](#)]
6. Akasofu, S.I.; Chapman, S. The Development of the Main Phase of Magnetic Storms. *J. Geophys. Res.* **1963**, *68*, 125–129. [[CrossRef](#)]
7. Gosling, J.T.; McComas, D.J.; Phillips, J.L.; Bame, S.J. Geomagnetic activity associated with earth passage of interplanetary shock disturbances and coronal mass ejections. *J. Geophys. Res.* **1991**, *96*, 7831–7839. [[CrossRef](#)]
8. Gopalswamy, N.; Yashiro, S.; Michalek, G.; Xie, H.; Lepping, R.P.; Howard, R.A. Solar source of the largest geomagnetic storm of cycle 23. *Geophys. Rev. Lett.* **2005**, *32*, L12S09. [[CrossRef](#)]
9. Chen, P.F. Coronal Mass Ejections: Models and Their Observational Basis. *Living Rev. Sol. Phys.* **2011**, *8*, 1. [[CrossRef](#)]
10. Joshi, N.C.; Bankoti, N.S.; Pande, S.; Pande, B.; Pandey, K. Relationship between interplanetary field/plasma parameters with geomagnetic indices and their behavior during intense geomagnetic storms. *New Astron.* **2011**, *16*, 366–385. [[CrossRef](#)]
11. Webb, D.F.; Howard, T.A. Coronal Mass Ejections: Observations. *Living Rev. Sol. Phys.* **2012**, *9*, 3. [[CrossRef](#)]
12. Telloni, D.; Antonucci, E.; Bemporad, A.; Bianchi, T.; Bruno, R.; Fineschi, S.; Magli, E.; Nicolini, G.; Susino, R. Detection of Coronal Mass Ejections at L1 and Forecast of Their Geoeffectiveness. *Astrophys. J.* **2019**, *885*, 120. [[CrossRef](#)]
13. Marchezi, J.P.; Dai, L.; Alves, L.R.; Da Silva, L.A.; Sibeck, D.G.; Lago, A.D.; Souza, V.M.; Jauer, P.R.; Veira, L.E.A.; Cardoso, F.R.; et al. Electron Flux Variability and Ultra-Low Frequency Wave Activity in the Outer Radiation Belt under the Influence of Interplanetary Coronal Mass Ejections and High-Speed Solar Wind Streams: A Statistical Analysis From the Van Allen Probes Era. *J. Geophys. Res. (Space Phys.)* **2022**, *127*, e29887. [[CrossRef](#)]
14. Schillings, A.; Palin, L.; Opgenoorth, H.J.; Hamrin, M.; Rosenqvist, L.; Gjerloev, J.W.; Juusola, L.; Barnes, R. Distribution and Occurrence Frequency of dB/dt Spikes During Magnetic Storms 1980–2020. *Space Weather* **2022**, *20*, e2021SW002953. [[CrossRef](#)]
15. Milan, S.E.; Imber, S.M.; Fleetham, A.L.; Gjerloev, J. Solar Cycle and Solar Wind Dependence of the Occurrence of Large dB/dt Events at High Latitudes. *J. Geophys. Res. (Space Phys.)* **2023**, *128*, e2022JA030953. [[CrossRef](#)]
16. Hapgood, M.; Liu, H.; Lugaz, N. SpaceX—Sailing Close to the Space Weather? *Space Weather* **2022**, *20*, e2022SW003074. [[CrossRef](#)]
17. Miteva, R.; Samwel, S.W.; Tkatchova, S. Space Weather Effects on Satellites. *Astronomy* **2023**, *2*, 165–179. [[CrossRef](#)]
18. McCuen, B.A.; Moldwin, M.B.; Steinmetz, E.S.; Engebretson, M.J. Automated High-Frequency Geomagnetic Disturbance Classifier: A Machine Learning Approach to Identifying Noise while Retaining High-Frequency Components of the Geomagnetic Field. *J. Geophys. Res. (Space Phys.)* **2023**, *128*, e2022JA030842. [[CrossRef](#)]
19. Loewe, C.A.; Pröls, G.W. Classification and mean behavior of magnetic storms. *J. Geophys. Res.* **1997**, *102*, 14209–14214. [[CrossRef](#)]
20. Mayaud, P.N. Derivation, Meaning, and Use of Geomagnetic Indices. *Geophys. Monogr. Ser.* **1980**, *22*, 607. [[CrossRef](#)]
21. Banerjee, A.; Bej, A.; Chatterjee, T.N. On the existence of a long range correlation in the Geomagnetic Disturbance storm time (Dst) index. *Astrophys. Space Sci.* **2012**, *337*, 23–32. [[CrossRef](#)]
22. Borovsky, J.E.; Shprits, Y.Y. Is the Dst Index Sufficient to Define All Geospace Storms? *J. Geophys. Res. (Space Phys.)* **2017**, *122*, 11543–11547. [[CrossRef](#)]
23. Bartels, J.; Veldkamp, J. International data on magnetic disturbances, fourth quarter, 1953. *J. Geophys. Res.* **1954**, *59*, 297–302. [[CrossRef](#)]
24. Matzka, J.; Stolle, C.; Yamazaki, Y.; Bronkalla, O.; Morschhauser, A. The Geomagnetic Kp Index and Derived Indices of Geomagnetic Activity. *Space Weather* **2021**, *19*, e2020SW002641. [[CrossRef](#)]
25. McPherron, R.L. Determination of linear filters for predicting Ap during Jan. 1997. *Geophys. Rev. Lett.* **1998**, *25*, 3035–3038. [[CrossRef](#)]
26. Kamide, Y.; Rostoker, G. What Is the Physical Meaning of the AE Index? *EOS Trans.* **2004**, *85*, 188–192. [[CrossRef](#)]
27. Lakhina, G.S.; Tsurutani, B.T. Geomagnetic storms: Historical perspective to modern view. *Geosci. Lett.* **2016**, *3*, 5. [[CrossRef](#)]
28. Tsurutani, B.T.; Gonzalez, W.D.; Lakhina, G.S.; Alex, S. The extreme magnetic storm of 1–2 September 1859. *J. Geophys. Res. (Space Physics)* **2003**, *108*, 1268. [[CrossRef](#)]
29. Lockwood, M.; Owens, M.J.; Barnard, L.A.; Scott, C.J.; Watt, C.E.; Bentley, S. Space climate and space weather over the past 400 years: 2. Proxy indicators of geomagnetic storm and substorm occurrence. *J. Space Weather Space Clim.* **2018**, *8*, A12. [[CrossRef](#)]
30. Temmer, M. Space weather: The solar perspective. *Living Rev. Sol. Phys.* **2021**, *18*, 4. [[CrossRef](#)]
31. Akasofu, S.I. A Historical Review of the Geomagnetic Storm-Producing Plasma Flows from the Sun. *Space Sci. Rev.* **2011**, *164*, 85–132. [[CrossRef](#)]
32. Manu, V.; Balan, N.; Zhang, Q.H.; Xing, Z.Y. Association of the Main Phase of the Geomagnetic Storms in Solar Cycles 23 and 24 with Corresponding Solar Wind-IMF Parameters. *J. Geophys. Res. (Space Phys.)* **2022**, *127*, e2022JA030747. [[CrossRef](#)]

33. Burton, R.K.; McPherron, R.L.; Russell, C.T. An empirical relationship between interplanetary conditions and Dst. *J. Geophys. Res.* **1975**, *80*, 4204. [[CrossRef](#)]
34. Gopalswamy, N. Solar connections of geoeffective magnetic structures. *J. Atmos. Sol.-Terr. Phys.* **2008**, *70*, 2078–2100. [[CrossRef](#)]
35. Samwel, S.; Miteva, R. Correlations between space weather parameters during intense geomagnetic storms: Analytical study. *Adv. Space Res.* **2023**, *72*, 3440–3453. [[CrossRef](#)]
36. Vennerstrom, S.; Lefevre, L.; Dumbović, M.; Crosby, N.; Malandraki, O.; Patsou, I.; Clette, F.; Veronig, A.; Vršnak, B.; Leer, K.; et al. Extreme Geomagnetic Storms—1868–2010. *Sol. Phys.* **2016**, *291*, 1447–1481. [[CrossRef](#)]
37. Balan, N.; Zhang, Q.H.; Xing, Z.; Skoug, R.; Shiokawa, K.; Lühr, H.; Tulasi Ram, S.; Otsuka, Y.; Zhao, L. Capability of Geomagnetic Storm Parameters to Identify Severe Space Weather. *Astrophys. J.* **2019**, *887*, 51. [[CrossRef](#)]
38. Richardson, I.G.; Webb, D.F.; Zhang, J.; Berdichevsky, D.B.; Biesecker, D.A.; Kasper, J.C.; Kataoka, R.; Steinberg, J.T.; Thompson, B.J.; Wu, C.C.; et al. Major geomagnetic storms ( $Dst \leq -100$  nT) generated by corotating interaction regions. *J. Geophys. Res. (Space Phys.)* **2006**, *111*, A07S09. [[CrossRef](#)]
39. Dumitrache, C.; Popescu, N.A. The solar cycle 24 geomagnetic storms triggered by ICMEs and CIRs. *Rom. Astron. J.* **2018**, *28*, 177–186.
40. Choraghe, K.; Shaikh, Z.; Raghav, A.; Ghag, K.; Dhamane, O. Intense ( $SYM - H \leq -100$  nT) geomagnetic storms induced by planar magnetic structures in co-rotating interaction regions. *Adv. Space Res.* **2023**, *72*, 3220–3228. [[CrossRef](#)]
41. Zhang, J.; Richardson, I.G.; Webb, D.F.; Gopalswamy, N.; Huttunen, E.; Kasper, J.C.; Nitta, N.V.; Poomvises, W.; Thompson, B.J.; Wu, C.C.; et al. Solar and interplanetary sources of major geomagnetic storms ( $Dst \leq -100$  nT) during 1996–2005. *J. Geophys. Res. (Space Phys.)* **2007**, *112*, A10102. [[CrossRef](#)]
42. Miteva, R. On extreme space weather events: Solar eruptions, energetic protons and geomagnetic storms. *Adv. Space Res.* **2020**, *66*, 1977–1991. [[CrossRef](#)]
43. Miteva, R.; Samwel, S.W.; Nedal, M. Geomagnetic Storms and their Solar Origin in Solar Cycle 24 (2009–2019). In Proceedings of the XIII Bulgarian-Serbian Astronomical Conference, BSAC 2022, Velingrad, Bulgaria, 3–7 October 2022; Semkov, E., Dimitrijevic, M.S., Dechev, M., Simic, Z., Eds.; Astronomical Society “Rudjer Boskovic”: Belgrade, Serbia, 2023; pp. 125–135; ISBN 978-868903525-4
44. Miteva, R.; Samwel, S.W.; Costa-Duarte, M.V. The Wind/EPACT Proton Event Catalog (1996–2016). *Sol. Phys.* **2018**, *293*, 27. [[CrossRef](#)]
45. Samwel, S.W.; Miteva, R. Catalogue of in situ observed solar energetic electrons from ACE/EPAM instrument. *Mon. Not. R. Astron. Soc.* **2021**, *505*, 5212–5227. [[CrossRef](#)]
46. Kilpua, E.; Lugaz, N.; Mays, M.L.; Temmer, M. Forecasting the Structure and Orientation of Earthbound Coronal Mass Ejections. *Space Weather* **2019**, *17*, 498–526. [[CrossRef](#)]
47. Miteva, R.; Samwel, S.W.; Zabunov, S. Multi-Energy Proton Events and Geomagnetic Storms in Solar Cycles 23 and 24. In Proceedings of the SES-2020 Conference, Sofia, Bulgaria, 4–6 November 2020; pp. 64–68.
48. Mansilla, G.A. Solar wind and IMF parameters associated with geomagnetic storms with  $Dst < -50$  nT. *Phys. Scr.* **2008**, *78*, 045902. [[CrossRef](#)]

**Disclaimer/Publisher’s Note:** The statements, opinions and data contained in all publications are solely those of the individual author(s) and contributor(s) and not of MDPI and/or the editor(s). MDPI and/or the editor(s) disclaim responsibility for any injury to people or property resulting from any ideas, methods, instructions or products referred to in the content.